Received: 24 November 2022 | Revised: 17 February 2023 | Accepted: 20 February 2023

DOI: 10.1111/mpp.13324

Molecular Plant Pathology WILEY

ORIGINAL ARTICLE

Site-specific analysis reveals candidate cross-kingdom small RNAs, tRNA and rRNA fragments, and signs of fungal RNA phasing in the barley–powdery mildew interaction

Stefan Kusch | Mansi Singh | Hannah Thieron | Pietro D. Spanu | Ralph Panstruga

Unit of Plant Molecular Cell Biology, Institute for Biology I, RWTH Aachen University, Aachen, Germany

Correspondence
Pietro D. Spanu, Imperial College, London, UK.
Email: p.spanu@imperial.ac.uk

Present address
Pietro D. Spanu, Imperial College, London, UK

Funding information
Alexander von Humboldt-Stiftung, Grant/Award Number: GBR 1204122 GSA; Deutsche Forschungsgemeinschaft, Grant/Award Number: 433194101 and 274444799; Leverhulme Trust, Grant/Award Number: RF-2019-053

Abstract

The establishment of host–microbe interactions requires molecular communication between both partners, which may involve the mutual transfer of noncoding small RNAs. Previous evidence suggests that this is also true for powdery mildew disease in barley, which is caused by the fungal pathogen *Blumeria hordei*. However, previous studies lacked spatial resolution regarding the accumulation of small RNAs upon host infection by *B. hordei*. Here, we analysed site-specific small RNA repertoires in the context of the barley–*B. hordei* interaction. To this end, we dissected infected leaves into separate fractions representing different sites that are key to the pathogenic process: epiphytic fungal mycelium, infected plant epidermis, isolated haustoria, a vesicle-enriched fraction from infected epidermis, and extracellular vesicles. Unexpectedly, we discovered enrichment of specific 31–33-base 5′-terminal fragments of barley 5.8S ribosomal RNA in extracellular vesicles and infected epidermis, as well as particular *B. hordei* transfer RNA fragments in haustoria. We describe canonical small RNAs from both the plant host and the fungal pathogen that may confer cross-kingdom RNA interference activity. Interestingly, we found first evidence of phased small interfering RNAs in *B. hordei*, a feature usually attributed to plants, which may be associated with the posttranscriptional control of fungal coding genes, pseudogenes, and transposable elements. Our data suggest a key and possibly site-specific role for cross-kingdom RNA interference and noncoding RNA fragments in the host–pathogen communication between *B. hordei* and its host barley.

KEYWORDS
barley, *Blumeria*, cross-kingdom RNAi, extracellular vesicles, phased RNA, powdery mildew, small RNA

1 | INTRODUCTION

All complex multicellular organisms, including plants, not only require the exchange of information between cells for development and reproduction, but also need to communicate signals between each other and to coordinate the response to external stimuli. This exchange is referred to as either intra- or interorganismal communication, depending on whether it takes place between cells of the

same organism or between separate organisms. A special case of interorganismal communication is the exchange of information between organisms of different taxa. Examples of this phenomenon in the area of plant–microbe interactions comprise mutually advantageous symbioses and diseases caused by pathogenic fungi (Ma et al., 2019; Wong-Bajracharya et al., 2022). Gene regulation by noncoding small RNAs (sRNAs) can play an important role in the context of such plant–microbe encounters (Ma et al., 2019).

In plants, sRNAs are important for regulating and fine-tuning diverse processes, including growth and development, maintenance of genome integrity, epigenetic inheritance, and responses to both abiotic and biotic stress (Chen & Rechavi, 2022; Klesen et al., 2020). Based on their biogenesis and function, sRNAs can be divided into two major subclasses: microRNAs (miRNAs) and small interfering RNAs (siRNAs; Bologna & Voinnet, 2014). *MicroRNA* (*MIR*) genes encode pri-miRNAs, which are further processed into pre-miRNAs and finally mature miRNAs. In eukaryotes other than mammals and plants, such as fungi, it is challenging to prove the presence of bona fide miRNAs due to lack of evidence for the nonfunctional miRNA precursor strand; for this reason, they are termed miRNA-like RNAs (milRNAs; Lee et al., 2010). In contrast to miRNAs, siRNAs are generated from double-stranded RNA molecules of various origins (Bologna & Voinnet, 2014). In some cases, miRNAs trigger the generation of secondary siRNAs, for example phased siRNAs (phasiRNAs, i.e., regularly spaced siRNAs that derive from a common precursor RNA), which are sometimes associated with the silencing of transposable elements (Komiya, 2017). If the sRNA that triggers the formation of phasiRNAs is derived from a remote *trans*-acting sRNA locus, it is termed *trans*-acting siRNA (tasiRNA). While phasiRNAs and tasiRNAs are well described in plants, they are largely unexplored in fungi; to the best of our knowledge, only one study has reported their existence in the fungal kingdom (Lee Marzano et al., 2018).

Both classes of sRNAs can induce either transcriptional or posttranscriptional gene silencing of specific target genes, collectively referred to as RNA interference (RNAi; Fire et al., 1998). Irrespective of the class, biogenesis, and function of the sRNA, RNAi involves cleavage of a double-stranded RNA (dsRNA) molecule by a Dicer-like (Dcl) ribonuclease and loading of the mature sRNA onto an Argonaute (Ago) protein, together forming the RNA-induced silencing complex (Bologna & Voinnet, 2014). Dcl proteins process the dsRNA precursor fragments into smaller pieces of 21–24 nucleotides or bases. The length of the fragment produced depends on the specific Dcl proteins, which recognize different types of dsRNA. The fragments are then bound by Ago proteins that specifically distinguish different sRNA lengths and are associated with distinct modes of gene silencing. For example, *Arabidopsis thaliana* AGO1 binds 21-base miRNAs generated by DCL1 or DCL4 and executes posttranscriptional gene silencing by cleaving target mRNAs in a sequence-specific manner. By contrast, *A. thaliana* AGO4 binds almost exclusively 24-base siRNAs generated by DCL3. AGO4 then induces transcriptional gene silencing by triggering DNA methylation, a process referred to as RNA-dependent DNA methylation (Fukudome & Fukuhara, 2017). In each case, the Ago-bound sRNA determines target specificity through sequence complementarity and the Ago protein is the key effector for gene silencing. In the context of interorganismal communication, the phenomenon of sRNA-triggered *trans*-species gene silencing has been termed cross-kingdom RNAi. The function of sRNAs in cross-kingdom RNAi has been demonstrated for various interactions of plants with filamentous plant pathogens, such as cotton and *Verticillium dahliae* (Zhang et al., 2016) and *A. thaliana* and the downy mildew pathogen *Hyaloperonospora arabidopsidis* (Dunker et al., 2020). One of the best-studied systems for plant–microbe cross-kingdom RNAi is the *A. thaliana*–*Botrytis cinerea* pathosystem, where exchange of sRNAs occurs in both directions (Wang et al., 2016; Weiberg et al., 2013). Once fungal sRNAs reach plant cells, they are loaded onto *A. thaliana* Ago proteins, which carry out the cleavage of host target transcripts such as those encoding mitogen-activated protein kinases (Weiberg et al., 2013). Similarly, the most abundant *A. thaliana* sRNAs detected in *B. cinerea* cells originate from tasiRNAs or intergenic loci, and target fungal genes important for pathogenicity (Cai et al., 2018). Intriguingly, phasiRNAs can be found in extracellular vesicles (EVs) of *A. thaliana* plants and contribute to resistance against the filamentous pathogen *Phytophthora capsici*. The *Phytophthora. sojae* effector PSR2 prevents phasiRNA synthesis, rendering *A. thaliana* susceptible to infection (Hou et al., 2019).

EVs may thus serve as shuttles for inter- and intraorganismal RNA molecule transfer in the context of plant–microbe interactions (Cai et al., 2018). The release of EVs and their contents into the plant apoplast upon pathogen challenge and their delivery to infection sites was first described over 50 years ago (He et al., 2021; Manocha & Shaw, 1964). This parallels the situation in mammalian cells, where EVs in the intercellular space target nearby and distant cells and are important components of intra-organismal communication (Skokos et al., 2001). The EVs interact with recipient cells to deliver cargo like sRNAs by membrane fusion and vesicle internalization (Morelli et al., 2004; Parolini et al., 2009; Segura et al., 2007). EVs occur in all prokaryotic and eukaryotic phyla (Woith et al., 2019). However, it is still unclear whether EV shuttling is the main mechanism for the delivery of sRNAs in plant–pathogen interactions, because evidence for the shuttling of sRNAs outside of EVs was recently found in *A. thaliana* (Zand Karimi et al., 2022).

The agronomically important crop barley (*Hordeum vulgare*) is the host plant of the ascomycete fungus *Blumeria hordei*, previously named *B. graminis* f. sp. *hordei* (Liu et al., 2021), which causes powdery mildew disease in barley. *B. hordei* colonizes barley biotrophically and the obligate relationship between host and pathogen requires tightly controlled gene regulation. In a previous study, we found that the essential components of the RNAi machinery are present in *B. hordei* (Kusch et al., 2018). Moreover, we discovered at least 1250 sRNA loci in the *B. hordei* genome, of which 524 were predicted to have mRNA targets in the host barley. Expression of sRNAs in both barley and *B. hordei* is consistent with a role in regulating transcript abundance in both partners during the interaction (Hunt et al., 2019). In *B. hordei*, milRNAs may control the mRNA levels of fungal virulence genes, whereas barley miRNAs and phasiRNAs might

control transcript levels of components of the plant innate immune system. Interorganismal exchange of RNAs is thought to be mediated by membrane-bound vesicles (Cai et al., 2018). Interestingly, vesicle-like structures have been observed at the interface between *B. hordei* infection structures and barley leaf epidermal cells (An et al., 2006; Hippe, 1985); this finding would be consistent with an exchange of sRNAs mediated by EVs in the context of the barley–powdery mildew interaction.

In this study, we analysed the sRNA spectrum in the *B. hordei*–barley pathosystem. To this end, we dissected infected leaves into separate fractions representing different sites that are key to the pathogenic process, that is, epiphytic fungal mycelium, infected plant epidermis, isolated haustoria, a vesicle-enriched fraction from infected epidermis, and EVs. Unexpectedly, we discovered enrichment of specific 31–33-base 5′-fragments of barley 5.8S ribosomal RNA (rRNA) in EVs, vesicles, and infected epidermis, as well as specific *B. hordei* transfer RNA (tRNA) fragments in haustoria. We describe canonical sRNAs from both the plant host and the fungal pathogen that may confer cross-kingdom RNAi activity. Interestingly, we found first evidence of phasiRNAs in *B. hordei*, a feature usually attributed to plants, which may be associated with the posttranscriptional control of coding genes, pseudogenes, and transposable elements. Our data suggest a key role for cross-kingdom RNAi and noncoding RNA fragments in the host–pathogen communication between *B. hordei* and its host barley.

2 | RESULTS

2.1 | Site-specific sRNA sampling

Based on three independent experiments, we isolated total RNA from the following biological materials ("sites") of *B. hordei*-infected barley leaves at 4 days after inoculation (Figure 1, see Experimental procedures for a detailed description of the samples): (1) epiphytic fungal mycelium (MYC), (2) infected epidermis without mycelium (EPI), (3) fungal haustoria (HAU), and (4) microsomes of the epidermis without mycelium (P40). In addition, RNA from (5) crude apoplastic EVs (EV+) were isolated from *B. hordei*-infected barley leaves at 3 days after inoculation. As a control, we also isolated (6) total RNA from crude EVs of noninfected plants (EV−). The 18 RNA samples (six sources, three replicates each) were then used to extract RNA, which was subsequently subjected to Illumina-based short read sequencing (sRNA-seq) at a depth of 30 million (MYC, EPI, HAU, P40) or 20 million (EV+, EV−) reads per sample (Table S1).

2.2 | Distinct rRNA- and tRNA-derived sRNAs are enriched in *B. hordei*- and barley-derived sample materials

The length of the trimmed sRNA reads ranged from 15 to 75 bases. However, the majority of the reads were between 15 and 40 bases long; between 282,734 (2.4%) and 5,432,088 (13.8%) reads per sample cumulatively accounted for reads of 41–74 bases (Table S2). We determined the sRNA length distribution profiles of the 15–40-base reads of the various samples and found that each of the six biological materials showed a distinctive and largely reproducible pattern: the sRNAs from mycelium (MYC) exhibited a bimodal distribution with a prominent peak at 21 and 22 bases, and a much shallower and broader peak with a maximum at 29–33 bases. Likewise, the epidermal (EPI) samples had a bimodal size distribution with marked peaks at 21–22 and 32–33 bases. The HAU and P40 samples exhibited a broad size range without any outstanding peak, but an increase in the number of 27–32-base reads compared to reads below or above this range. Finally, the two EV sample types (EV− and EV+) exhibited distinctive profiles: the EV+ size distribution was reminiscent of EPI and MYC samples, with a bimodal distribution and characteristic peaks at 21–23 and 31–32 bases while the EV− sRNAs showed a single prominent peak at 31–32 bases (Figure S1a).

We mapped the sRNA reads to the respective reference genomes of *H. vulgare* IBSCv2 (Mascher et al., 2017) and *B. hordei* DH14 (Frantzeskakis et al., 2018) using bowtie within the ShortStack (Johnson et al., 2016) pipeline. Overall, between 3,715,684 and 32,777,442 reads could be assigned to the *H. vulgare* genome and between 431,626 and 22,069,070 reads to the *B. hordei* genome (Table S1). We next determined the number of reads mapping to each of the genomes separately for the read sizes of 15–40 bases (Figure S1b; Tables S3 and S4). We noted that reads below 19 bases could not be unequivocally allocated to either organism by read mapping alone (Figure S1c). Hence, we considered reads of <19 bases as ambiguous and disregarded these from further read length-related analysis, and we also removed any ambiguous reads of ≥19 bases from the analysis. We found that the majority of 21–22-base reads in the MYC and EPI samples unambiguously derived from the *B. hordei* genome, while reads from the 31–32- and 32–33-base peaks in the EPI and EV samples almost exclusively aligned to the genome of *H. vulgare*. The majority of reads of >19 bases from the P40 and EV− samples were from the *H. vulgare* genome, while reads from the EPI, HAU, and EV+ samples originated from both organisms. Regardless of the read length, except for the distinct 31–33-base peak in reads from *H. vulgare*, the majority of the reads originated from either coding genes or transposable elements (Figure S2).

We next explored the identity and possible molecular origin of the sRNAs from the very prominent 31–32-base peak in the EV+ samples and the 32–33-base peak in the EPI samples, both from *B. hordei*-infected barley leaves. Using MMSeqs2 for BLAST searches against the RNA families (RFAM) databases of conserved noncoding RNAs (i.e., tRNAs, rRNAs, small nucleolar RNAs, small nuclear RNAs), we found that >80% of the sequences in these two sample types corresponded to a specific short fragment of the barley 5.8S rRNA (Figure 2). This 5.8S rRNA fragment (rRF) was specifically found in 31–32-base reads in EV+ and EV− and in 32–33-base reads in EPI (Figure S3). In case of the P40 and HAU samples, only <15% of the reads originate from the barley 5.8S rRF. Between 15% and 30% of the reads in the MYC and HAU samples were identified as derived

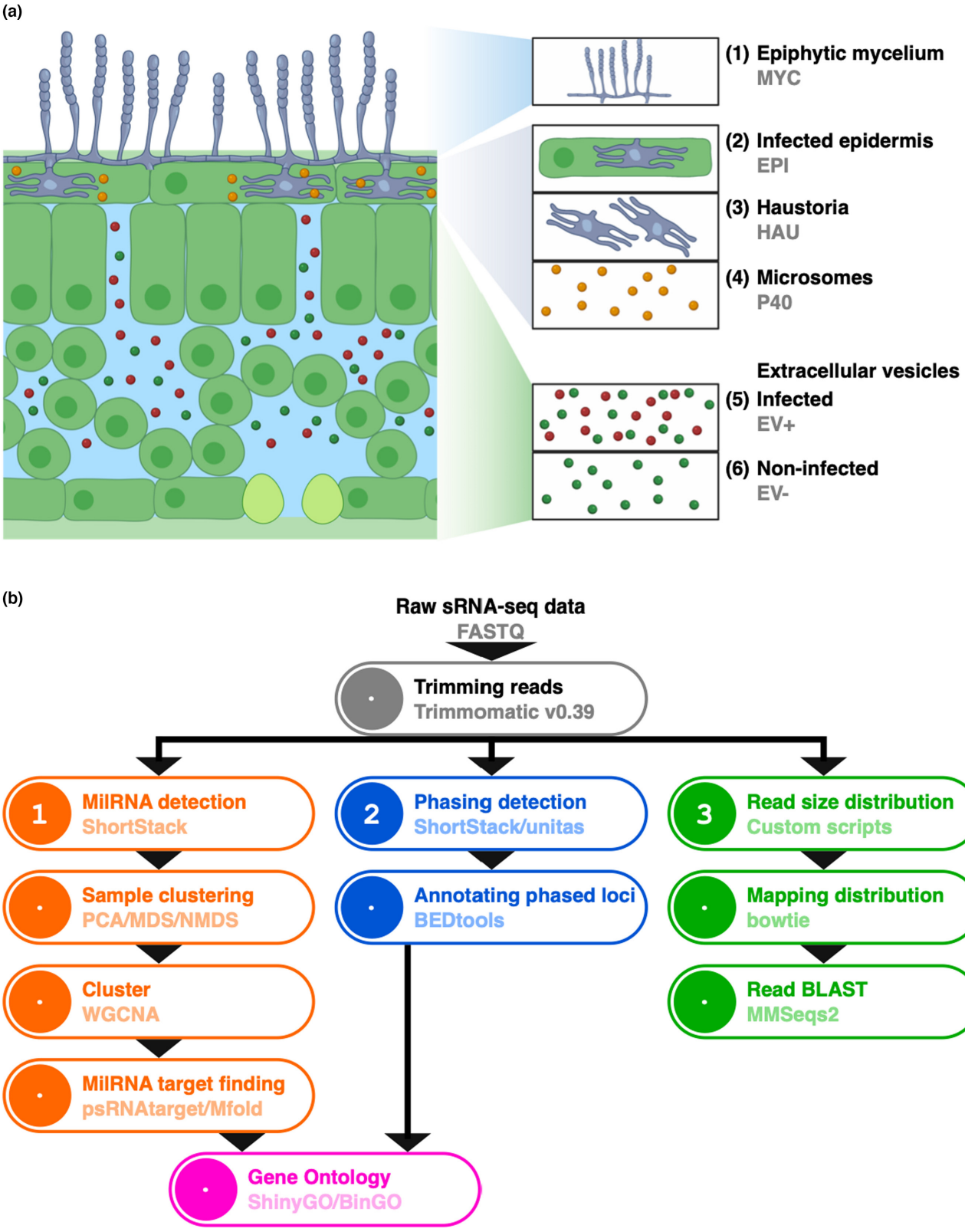

FIGURE 1 Isolation of total RNA from six distinct sample types. (a) We isolated total RNA from the following biological materials of *Blumeria hordei*-infected barley leaves at 4 days after inoculation: (1) epiphytic fungal mycelium (MYC), (2) infected epidermis without mycelium (EPI), (3) fungal haustoria (HAU), and (4) microsomes of the epidermis depleted of haustoria (P40). In addition, we isolated total RNA from (5) apoplastic extracellular vesicles of infected plants (EV+) at 3 days after inoculation and (6) apoplastic extracellular vesicles from noninfected control plants (EV−). The figure was created using bioRender.com. (b) Bioinformatic pipeline for sRNA-seq data analysis. We analysed the sRNA-seq reads in three ways: (1) by read size and read mapping distribution to the respective genomes, followed by read BLAST searches against the RFAM database for particular fractions of the read data; (2) by ShortStack analysis to detect putative milRNAs in both organisms, followed by principal component analysis (PCA) for sample clustering, milRNA expression analysis, milRNA target prediction, and functional description of these targets by gene ontology (GO) assignment; and (3) by detection of loci enriched with predicted phasiRNAs.

from *B. hordei* 5.8S rRNA (Figure 2). In HAU, *B. hordei* 5.8S rRFs were abundant in reads of 27–32 bases in length (Figure S3). Notably, the vast majority (>90%) of the 5.8S rRNA-associated reads mapped to the 3′ end of the molecule in both organisms, even in samples lacking a distinctive peak at 31–33 bases (Figure 2b and Table 1). We refer to these regions as *H. vulgare* rRF *Hvu*-rRF0001 and *B. hordei* rRF *Bho*-rRF0001 (Figure 2b and Table 2). In case of *B. hordei*, we found a second less abundant fragment adjacent to *Bho*-rRF0001, called *Bho*-rRF0002 (Figure S3 and Table 2).

In the P40 and HAU samples, which had a broad peak at 27–32 bases (Figure S1), a large portion of reads was identified as 28S (large subunit [LSU]) rRNA-derived sRNAs (Figures 2 and S3). P40 had >60% of barley 28S rRNA-originating reads, while HAU reads could be mapped to >25% of barley and >20% of *B. hordei* 28S rRNA sequences. We aligned these reads in a targeted manner to the 28S LSU rRNAs of *H. vulgare* and *B. hordei* and noted distinct prominent peaks, suggesting the enrichment of specific 28S rRFs in *B. hordei*-infected barley plants (Figures S4 and S5, Tables S5 and S6). In case of the barley 28S rRNA, the first peak was approximately at position 2100–2150 (*Hvu*-rRF0002) and the second peak around position 3760–3800 (*Hvu*-rRF0003); both peaks were distinctive in the HAU and P40 samples. However, the samples EPI, EV+, and EV− lacked any such prominent signatures for the *H. vulgare* 28S rRNA. For *B. hordei*, the 28S rRNA-derived sRNAs mapped to a peak at position

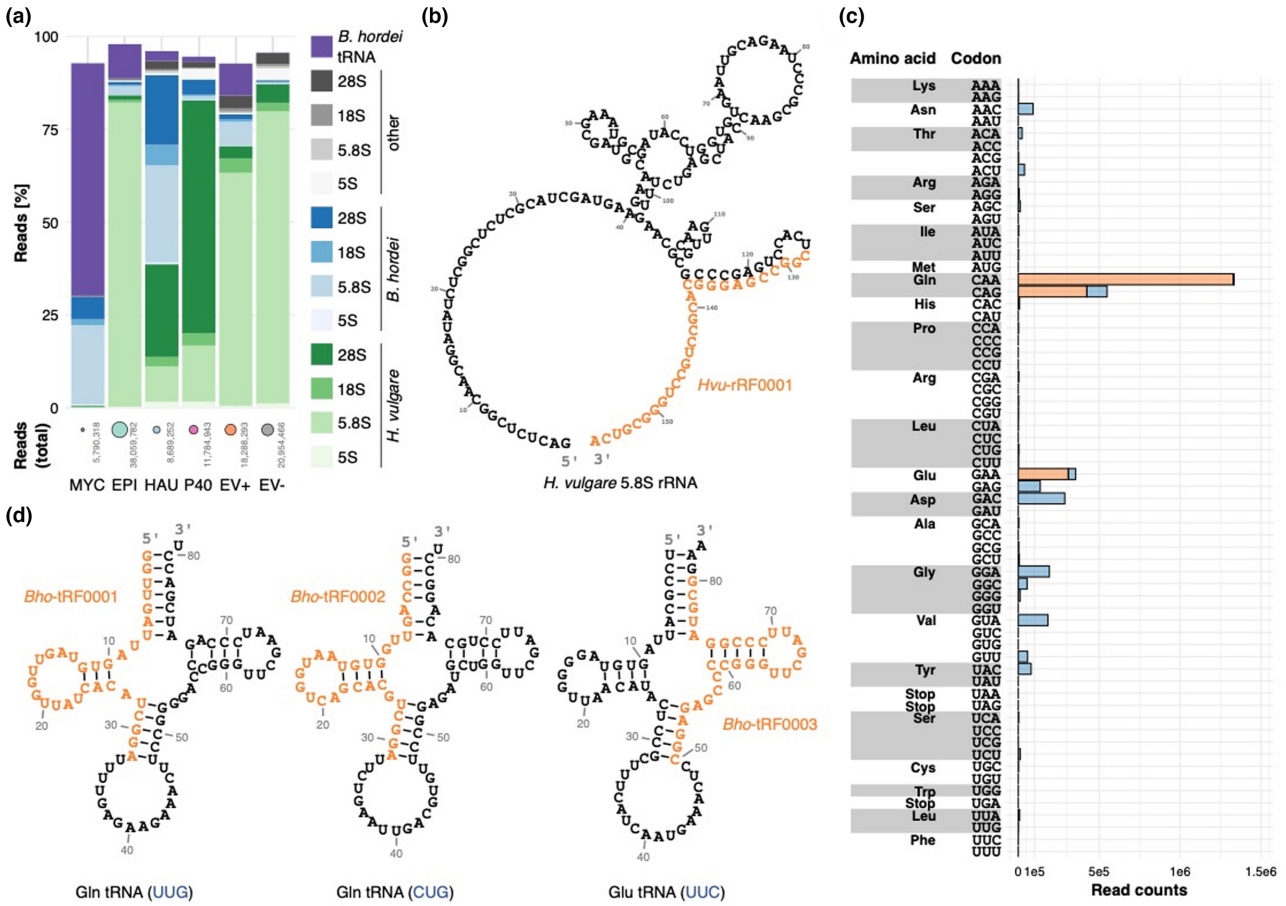

FIGURE 2 Specific barley 5.8S rRNA- and *Blumeria hordei* tRNA-derived sRNAs are enriched in 31–33-base reads. We aligned sRNA-seq reads of 31–33 bases in length to the RFAM database using MMSeqs2 (Steinegger & Söding, 2017). (a) The stacked bar graph shows the percentage of reads identified as 5S, 5.8S, 18S (small subunit [SSU]), 28S (large subunit [LSU]), or tRNA, as indicated in the colour-coded legend. Green, reads identified as derived from *Hordeum vulgare*; blue, reads identified as derived from *B. hordei* DH14; grey, reads not assigned to either *H. vulgare* or *B. hordei*; purple, reads identified as *B. hordei* tRNA-derived. Six sample types were analysed: epiphytic fungal mycelium (MYC), infected epidermis without mycelium (EPI), fungal haustoria (HAU), microsomes of the epidermis without haustoria (P40), apoplastic extracellular vesicles (EV+), and apoplastic extracellular vesicles of noninfected control plants (EV−). The total number of reads assigned to each sample is given below the bar graph (visualized by circle size). (b) Predicted secondary structure of the barley 5.8S rRNA (RFAM accession CAJW010993076.1:c203-48; RNAcentral accession URS0000C3A4AE_112509), calculated by R2DT in RNAcentral (https://rnacentral.org) and visualized with Forna (Kerpedjiev et al., 2015). The RNA sequence in orange indicates the over-represented 3′ end in the reads from the EPI and EV+ samples. (c) Histogram showing the number of reads (read counts, *x*-axis) accounting for the *B. hordei* tRNA-derived reads in the sample MYC. The 20 amino acids according to the standard genetic code and respective mRNA codons are indicated on the left. The orange portion of the histogram bars indicates the fraction of reads coming from the three most abundant tRNA fragments. (d) The three most abundant tRNAs represented in the MYC sample are shown; left, Gln tRNA with UUG anticodon; middle, Gln tRNA with CUG anticodon; right, Glu tRNA with UUC anticodon. The orange-labelled sequences indicate the abundant tRNA fragments.

TABLE 1 *Hordeum vulgare* and *Blumeria hordei* sRNAs (rRFs) derived from the 3′ end of the respective 5.8S rRNA.

			H. vulgare			*B. hordei*		
Sample[a]	Peak (bases)	Number of reads	5.8S rRNA	3′-fragment *Hvu*-rRF0001	%	5.8S rRNA	3′-fragment *Bho*-rRF0001	%
MYC	31–32	5,667,110	4,984	4,719	94.7	1,210,651	1,205,821	99.6
EPI	32–33	37,604,028	30,810,544	30,592,716	99.3	888,803	831,512	93.4
HAU	31–32	8,489,360	809,111	763,391	94.3	2,218,412	1,740,772	78.5
P40	31–32	11,704,109	1,765,971	1,573,893	89.1	135,087	56,148	41.6
EV+	31–32	18,288,293	11,482,523	11,214,952	97.7	1,166,538	1,132,561	97.1
EV−	31–32	20,954,466	16,486,325	16,279,540	98.7	99,432	92,250	92.3

[a]MYC, epiphytic fungal mycelium; EPI, infected epidermis without mycelium; HAU, fungal haustoria; P40, microsomes of the epidermis without haustoria; EV+, apoplastic extracellular vesicles; EV−, apopplastic extracellular vesicles of noninfected control plants.

TABLE 2 Characteristic *Hordeum vulgare* and *Blumeria hordei* RNA fragments derived from tRNA (tRFs) and rRNA (rRFs).

Fragment	Sequence (5′–3′)	Species	RNA	Sample[a]
Hvu-rRF0001	CGGCCGAGGGCACGCCUGCCUGGGCGUCA	*H. vulgare*	5.8S rRNA	EPI, EV+, EV−
Hvu-rRF0002	CCGGAGGUAGGGUCCAGUGGCCGGAAGAGCA	*H. vulgare*	28S rRNA	HAU, P40
Hvu-rRF0003	CGCGACGGGGCAUUGUAAGUGGCAGAGUGGCC	*H. vulgare*	28S rRNA	EPI
Bho-rRF0001	UUCCCAGGGGCAUGCCUGUUCGAGCGUCC	*B. hordei*	5.8S rRNA	HAU
Bho-rRF0002	UCUUUGAACGCACAUUGCGCCCCUGGGA	*B. hordei*	5.8S rRNA	HAU
Bho-rRF0003	GUUACGGGCCCGAGUUGUAAUUUGUAGAAGAU	*B. hordei*	28S rRNA	MYC, EPI, HAU
Bho-rRF0004	AAGCGUGUUACCCAUACUUCACCGCCCGGGUA	*B. hordei*	28S rRNA	HAU, P40
Bho-tRF0001	GGUUGAUUAGUGUAGUUGGUUAUCACAUCGGA	*B. hordei*	tRNA	MYC
Bho-tRF0002	GGCCAGUUGGUGUAAUGGUCAGCACGUCGGA	*B. hordei*	tRNA	MYC
Bho-tRF0003	CGGAGAGCCCCGGGUUCGAUUCCCGGAUGCG	*B. hordei*	tRNA	MYC

[a]MYC, epiphytic fungal mycelium; EPI, infected epidermis without mycelium; HAU, fungal haustoria; P40, microsomes of the epidermis without haustoria; EV+, apoplastic extracellular vesicles; EV−, apopplastic extracellular vesicles of noninfected control plants.

430–470 (*Bho*-rRF0003), which is distinctive in the EPI, HAU, and MYC samples. In addition, a second peak at position 1620–1660 (*Bho*-rRF0004) appeared in the HAU and P40 samples.

More than 60% (3,557,695) of the reads from the MYC samples were identified as *B. hordei* tRNA-derived sRNAs (tRNA fragments [tRFs]; Figure 2). Intriguingly, >48% of these appear to originate from *B. hordei* tRNAs with anticodons for glutamine (Gln) (Figure 2d). The 5′ moiety of the UUG anticodon Gln tRNA accounted for 1,332,676 reads (37%), 424,142 reads (11.9%) were from the 5′ end and 124,372 (3.5%) from the 3′ end of the CUG anticodon Gln tRNA, and 314,017 reads (8.8%) were identified as the 3′ moiety of the UUC anticodon Glu tRNA. Next, we predicted the putative secondary structures and minimum free energy (MFE) values of the rRFs and tRFs using the Vienna RNAfold web server (Gruber et al., 2008) to assess if they would be thermodynamically stable (Table S7). Notably, *Hvu*-rRF0001 was predicted to form a secondary structure that was particularly stable, forming two double-stranded helices at a free energy of −11.9 kcal/mol (Figure S6). This was markedly more stable than any other theoretical fragment that could be derived from the barley rRNA (between −1.5 and −4.7 kcal/mol) and also than the *B. hordei* 5.8S rRNA-derived fragments (−5.3 and −3.4 kcal/mol, respectively). However, not all abundant rRFs exhibited low free energy (range between −2.4 and −11.9 kcal/mol; Table S7). Similarly, the predicted secondary structures of the *B. hordei* tRFs ranged from −1.7 to −10.4 kcal/mol free energy, overall suggesting that the tRFs and rRFs we observed (Table 2; File S1) may assume secondary structures that are thermodynamically stable, but calculated free energy is insufficient evidence to explain the high abundance of most fragments in our dataset.

To assess if specific rRFs occur frequently in infected plants, we then mined publicly available sRNA sequencing datasets from barley, wheat (*Triticum aestivum*), soybean (*Glycine max*), and *Arabidopsis thaliana* under various biotic and abiotic stresses (see Table S8 for all accessions). These data showed that read length distributions varied between experiments even within the same species (Figure S7). Notably, we did not find striking rRNA enrichment in response to infection or abiotic stress in this subset of sequencing data (Figure S8). The fact that another *B. hordei* sRNA-seq dataset (Hunt et al., 2019) also lacks evidence for abundant rRNA suggests that these fragments either appear late in infection (3–4 days postinoculation in our samples versus 48 h postinoculation in Hunt et al., 2019) or are only detectable in sampling material enriched with infected host cells. Altogether we identified distinctive barley 5.8S, 28S (both barley and *B. hordei*), and *B. hordei* tRNA-derived sRNAs enriched in *B. hordei*-infected barley samples (Table 2).

2.3 | Identification of milRNA genes in *B. hordei* and in barley

Next, we used the ShortStack pipeline to annotate and quantify our sRNA samples. Because bona fide miRNAs are difficult to predict in fungi (Lee et al., 2010), we identified milRNAs, which satisfy all conditions of miRNAs except detection of the precursor strand. Cumulatively, we identified 2711 unique *B. hordei* and 35,835 unique barley milRNA loci with this pipeline, accounting for 2558 and 29,987 unique milRNA sequences, respectively (Table S9; Files S2–S5). Of these, 3 *B. hordei* milRNAs and 59 barley sequences were classified as bona fide miRNAs by ShortStack. For *B. hordei*, most milRNAs were detected in the EPI, MYC, HAU, and EV+ samples (more than 200 milRNAs each), reflecting the abundance of fungal reads in these samples. In case of *H. vulgare*, EPI and MYC samples represented the largest numbers of milRNAs (more than 5000 each), followed by the EV−, HAU, and P40 samples.

Then, we determined read counts for milRNA loci in both *H. vulgare* and *B. hordei* using the read mapping information from ShortStack (Tables S10 and S11). We analysed sample relatedness by using non-metric multidimensional scaling (NMDS), which collapses multidimensional information into few dimensions (two in this case; Figure 3). In case of *H. vulgare*, the three replicates of MYC, EPI, HAU, and P40 each formed distinct clusters, while the EV+ samples were distinct but only broadly clustered, suggesting stronger variation between replicates. EV− samples did not show clear clustering, as two data points were similar to the EPI and MYC samples, and one was similar to the EV+ samples (Figure 3a). The replicates distributed similarly in the case of the *B. hordei* samples, but P40 samples showed a broader distribution and some overlap with the EV+ sample (Figure 3b). The EV− samples were obtained from noninfected leaves; nevertheless, 1651 EV− reads mapped to *B. hordei* milRNA loci in total, suggesting a low level of contamination of fungal milRNA in this sample. For both *H. vulgare* and *B. hordei*, the samples showed comparable Pearson-based hierarchical clustering (Figure 3c,d) and clustering trends in principal component analysis (PCA; Figure S9); analysis of similarity (ANOSIM) testing confirmed significant sample differentiation in both *H. vulgare* and *B. hordei* ($p < 1e{-}4$). In case of EV− and EV+, we found that the individual replicates also varied in terms of total number of reads per sample and read length distribution profiles (Figure S10). The distinct 31–32-base peak was hardly visible in EV− replicate #1 and EV+ replicate #2. In EV+ replicate #2, the 31–32-base reads consisted of >25% *B. hordei* 5.8S rRNA-derived and >50% tRNA-derived sRNAs, which was a unique pattern among the six EV samples. Overall, the differences in read numbers and profiles between samples suggest that the sequencing depth and quality varied greatly between replicates, causing an overall low signal-to-noise ratio in the EV fractions.

2.4 | Site-specific accumulation of milRNAs

We performed weighted gene coexpression network analysis (WGCNA) to identify milRNAs associated with MYC, EPI, HAU, P40, and EV+ samples for 22,415 *H. vulgare* and 2711 *B. hordei* milRNAs, and then assigned 11,334 *H. vulgare* and 2325 *B. hordei* milRNAs as enriched in compartments with at least 2.5-fold abundance above the average. For *H. vulgare*, 2496 milRNAs were enriched in MYC, 1137 in EPI, 422 in HAU, 410 in P40, and 615 in EV+ (Figure 4a). In case of *B. hordei*, 519 milRNAs were enriched in MYC, 260 in EPI, 108 in HAU, 59 in P40, and 26 in EV+ (Figure 4b). The samples MYC and EPI also showed considerable overlap of equally abundant milRNAs, as 1009 *B. hordei* milRNAs and 3628 *H. vulgare* milRNAs were more frequent in both samples. Furthermore, 137 *B. hordei* milRNAs were associated with MYC, EPI, and HAU. We used psRNAtarget (Dai & Zhao, 2011) to predict RNAi targets of *H. vulgare* and *B. hordei* milRNAs. Overall, 3693 *H. vulgare* milRNAs had putative targets, that is, 10,488 endogenous and 1309 *B. hordei* unique transcripts (Figure 4). In total, 90 (6.8%) of the possible *B. hordei* target genes code for proteins with a predicted secretion peptide. In case of *B. hordei* milRNAs, we found that 1205 milRNAs could target 581 endogenous genes, 50 (8.6%) of which encode proteins with a predicted secretion peptide, and 1677 may target 1985 transcripts in the host *H. vulgare*. Notably, HAU-specific *B. hordei* milRNAs had 76 potential cross-kingdom targets in *H. vulgare*, but only 23 endogenous targets, indicating a tendency towards cross-kingdom targeting of host plant genes by HAU-specific *B. hordei* milRNAs (Figure S11). These milRNAs exhibited higher average abundance (837 transcripts per million [TPM] on average) than, for example, MYC-specific milRNAs (59 TPM on average) or all milRNAs (181 TPM on average). The *B. hordei* milRNAs enriched in HAU and P40 (23 milRNAs, 5768 TPM on average) exhibited a similar pattern, predicted to target altogether 12 *H. vulgare* genes and only 1 *B. hordei* gene.

We then performed global and subset-specific Gene Ontology (GO) enrichment analysis of the putative cross-kingdom milRNA targets (Figure 5; Tables S12 and S13). We found significant GO enrichment in three of the *H. vulgare* milRNA cross-kingdom *B. hordei* gene target sets (Figure 5a). Protein phosphorylation-related terms (GO:0006468 and GO:0016773) were enriched between 3.6- and 12.9-fold in all three of the milRNA cross-kingdom target sets ($p_{adj} < 0.05$; 21–116 targets out of 264 genes with the GO term); however, protein phosphorylation was also enriched in any random set of target genes of 250 *H. vulgare* milRNAs. "ATP binding" was 1.5-fold enriched ($p_{adj} < 0.0011$, 96/534 genes) in the predicted cross-kingdom targets of MYC- and EPI-specific *H. vulgare* milRNAs. Two GO terms relating to protein K63-linked deubiquitination (GO:0070536 and GO:0061578) were 80.9-fold enriched in the putative cross-kingdom targets of *H. vulgare* milRNAs enriched in MYC, EPI, and HAU ($p_{adj} < 0.05$); however, this was one of the two *B. hordei* genes annotated with this GO term. Only three *B. hordei* milRNA cross-kingdom target sets, containing MYC-specific, EPI-specific, or MYC- and EPI-specific milRNAs, showed significant enrichment of GO terms (Figure 5b). Two genes targeted by MYC- and EPI-specific milRNAs had the GO term "microtubule-severing ATPase activity" ($p_{adj} < 0.046$; 128.9-fold enrichment; 2/5 genes), while the term "vacuole" was 6.5-fold enriched in the same set ($p_{adj} < 0.004$; 10/497 genes). In the MYC-specific set, "ADP binding" was 6.2-fold enriched

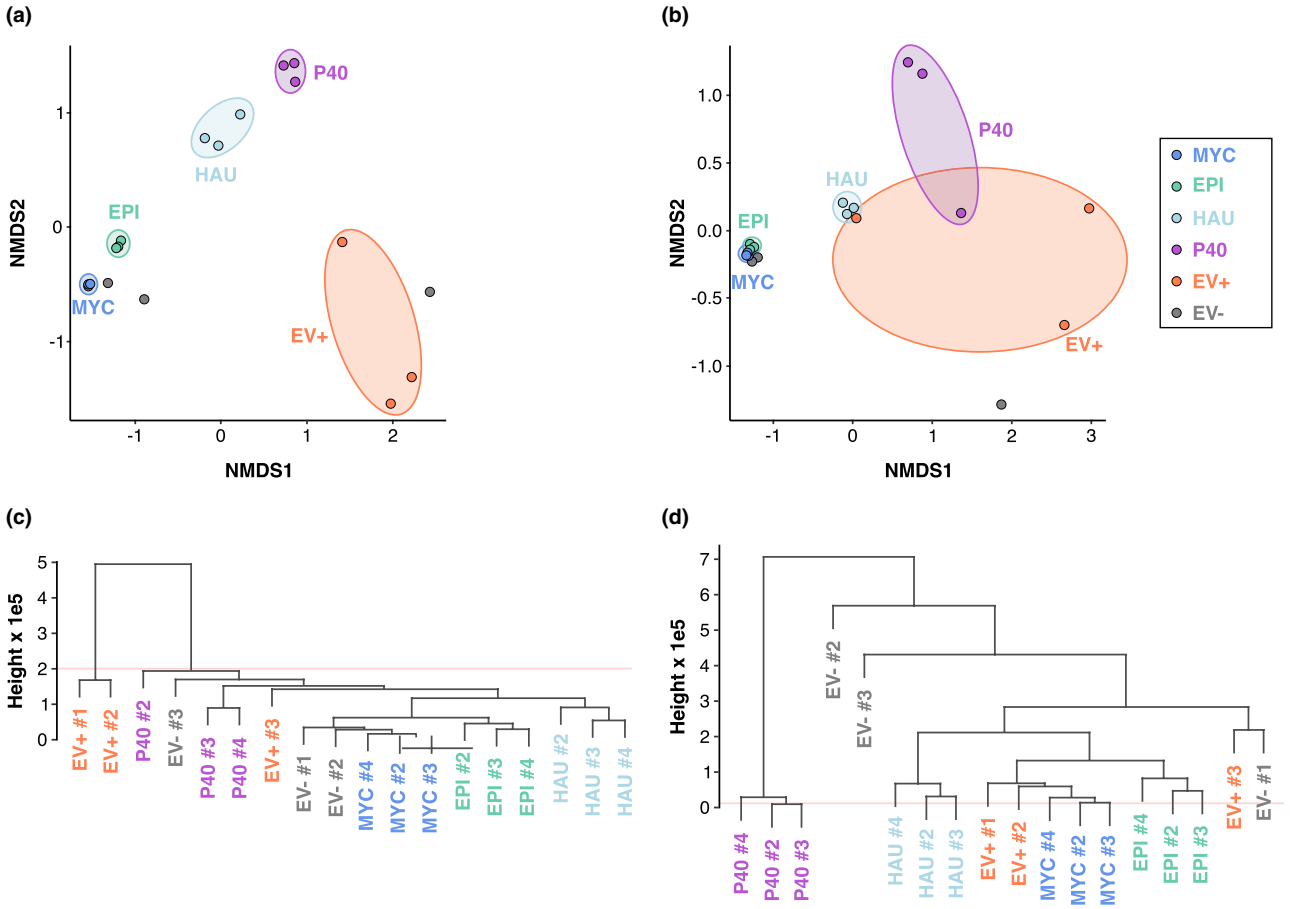

FIGURE 3 The milRNA content of microsomal samples differs from that of mycelial, epidermal, and haustorial samples. (a and b). We used nonmetric multidimensional scaling (NMDS), which collapses multidimensional information into two dimensions to visualize sample similarity. Each data point represents the collapsed milRNA expression data from *Hordeum vulgare* (a) and *Blumeria hordei* (b). Blue, epiphytic fungal mycelium (MYC); green, infected epidermis without mycelium (EPI); light blue, fungal haustoria (HAU); purple, microsomes of the epidermis without haustoria (P40); orange, apoplastic extracellular vesicles (EV+); grey, apoplastic extracellular vesicles of noninfected control plants (EV−). (c and d) milRNA sample distances based on a Pearson correlation matrix from the milRNA expression data. The pairwise Pearson correlations were used to calculate a Euclidean distance tree with all samples for *H. vulgare* (c) and *B. hordei* (d).

(p_{adj} < 0.04; 5/428 genes) and "nucleoside-triphosphatase activity" was 5.1-fold enriched (p_{adj} < 0.02; 8/839 genes); "ADP binding" was also enriched in the EPI-specific set (11-fold, p_{adj} < 0.009; 6/428 genes) but in random target gene sets of 250 milRNAs as well. The only GO terms enriched in endogenous milRNA targets of *B. hordei* were related to protein phosphorylation (Figure S12a), exhibiting 4-fold to 11-fold enrichment (p_{adj} < 7e−10; up to 24–50/264 genes) in MYC-, EPI-, MYC- and EPI-, and MYC/EPI/HAU-specific sets. Conversely, we found 69 enriched GO terms in the sets of putative endogenous *H. vulgare* target genes (Figure S12b; Tables S12 and S13). Many of these GO terms relate to regulatory, cell cycle, growth, and developmental processes.

Altogether, we detected that most *B. hordei* and *H. vulgare* milRNAs exhibited site-specific enrichment patterns, suggestive of their infection stage- and tissue-specific induction. Among the putative targets of *B. hordei* milRNAs, genes coding for proteins involved in protein phosphorylation appeared to be consistently overrepresented, both in presumed endogenous and cross-kingdom gene

FIGURE 4 Large sets of milRNAs exhibit site-specific distribution. (a and b) We calculated site-specific abundance in MYC, EPI, HAU, P40, and EV+ samples for (a) *Hordeum vulgare* and (b) *Blumeria hordei* using weighted gene coexpression network analysis (WGCNA) and assigned milRNAs to samples exhibiting >2.5-fold enrichment over the average. The bottom panels indicate the set sizes of milRNAs in the respective samples (bar graph, left); blue, epiphytic fungal mycelium (MYC); green, infected epidermis without mycelium (EPI); light blue, fungal haustoria (HAU); purple, microsomes of the epidermis without haustoria (P40); orange, apoplastic extracellular vesicles (EV+). The dots indicate the samples contributing to the respective interaction sets. The second panels from the bottom are bar graphs of the intersection numbers, which are the numbers of milRNAs in the exclusive intersections. The third panels from the bottom show the normalized abundance of the milRNAs in the respective interaction sets as violin plots; the maximum transcripts per million (TPM) value across samples was used for each data point. The top panels are stacked bar charts of the sum of predicted milRNA target genes in *B. hordei* (blue) and *H. vulgare* (green); *B. hordei* genes encoding a secreted protein are shown in orange.

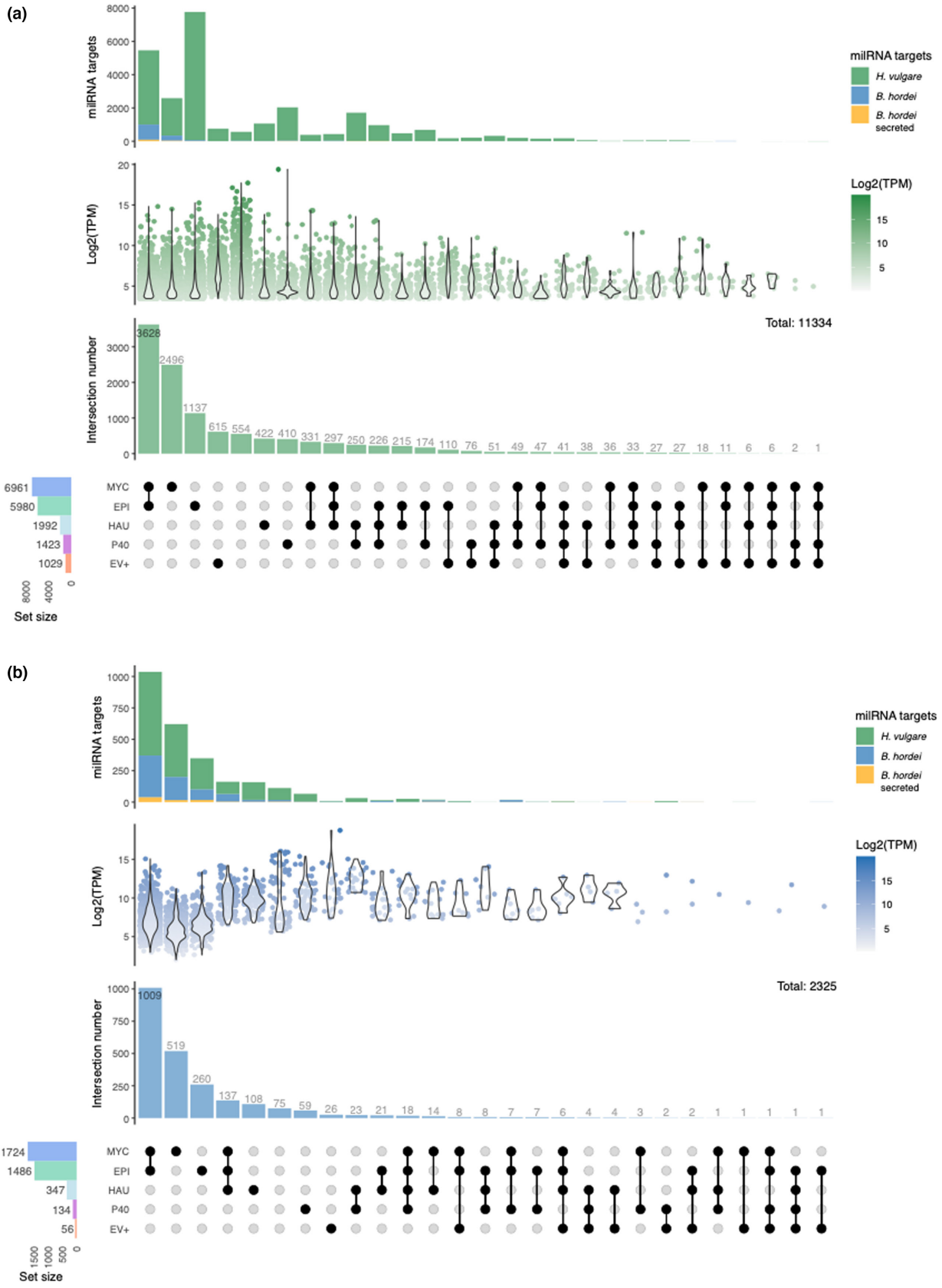

targets. However, this was also the case in random milRNA control sets, questioning the biological relevance of this observation. Predicted targets of *H. vulgare* milRNAs showed some enrichment of processes related to microtubule-severing ATPase activity in cross-kingdom *B. hordei* target genes, while endogenously regulating cell cycle, growth, and development.

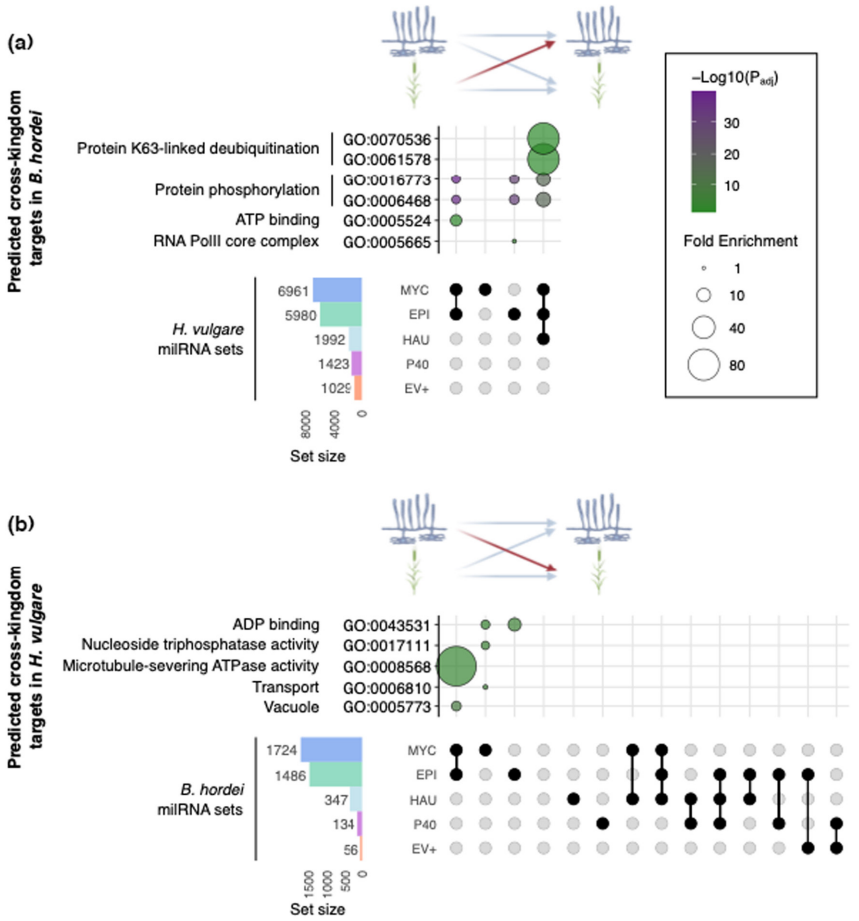

FIGURE 5 GO enrichment analysis of putative cross-kingdom milRNA targets. We determined all putative targets of the sets of *Blumeria hordei* and *Hordeum vulgare* milRNAs via psRNAtarget (Dai & Zhao, 2011). We used ShinyGO v. 0.75 (Ge et al., 2020) to calculate enriched gene ontology (GO) terms in all milRNA target sets and summarized redundant GO terms with EMBL-EBI QuickGO (https://www.ebi.ac.uk/QuickGO/) on GO v. 2022-04-26 and REVIGO (Supek et al., 2011). (a) Enriched GO terms found in putative cross-kingdom targets of *B. hordei* milRNAs in *H. vulgare*. (b) Enriched GO terms found in putative cross-kingdom targets of *H. vulgare* milRNAs in *B. hordei*. The GO terms and identifiers are indicated next to the bubble plots. Bubble size indicates fold enrichment of the term in the respective subset, fill colour indicates $-\log_{10}$(FDR-adjusted enrichment *p* value). The milRNA subsets are indicated below the bubble plots (see Figure 4 for all subsets). The icons on top of the plot were created with bioRender.com; the blue mycelium indicates *B. hordei* and the green plant barley.

2.5 | Phasing of *B. hordei* sRNA in coding genes and retrotransposons

In addition to predicting milRNA candidates, ShortStack (Johnson et al., 2016) can suggest loci containing phasiRNAs. Unexpectedly, ShortStack detected phasiRNAs from 22 *B. hordei* loci in our dataset, present in samples EPI and MYC but none of the other samples (phasing score > 30). Of these, two were found in genes encoding Sgk2 kinases (*BLGH_05411* and *BLGH_03674*), which are abundant in the genome of the fungus (Kusch et al., 2014), including at least one apparent pseudogenized Sgk2 kinase (*BLGH_03674*; Figures 6 and S13). Another four phasing loci corresponded to coding genes, namely *BLGH_02275*, *BLGH_00530*, *BLGH_00532* (encoding proteins of unknown function), and *BLGH_03506* (encoding CYP51/eburicol 14-α-demethylase, involved in ergosterol biosynthesis). The remaining 16 phasing loci were found to be in retrotransposons (Table S14). Because ShortStack is not optimized for phasiRNA prediction (Johnson et al., 2016), we used the PHASIS pipeline (Kakrana et al., 2017), unitas (Gebert et al., 2017), and PhaseTank (Guo et al., 2015) to detect evidence of phasing in the genome of *B. hordei* with our sRNA-seq dataset. PhaseTank failed to predict any phasiRNAs with our data. However, we detected 153 putative phasing loci with PHASIS, consisting of 21- or 22-base phasiRNAs ($p < 0.0005$, Table S14). We found that nine of these phasiRNA loci were located in coding genes of *B. hordei*, of which seven encode Sgk2 kinases. Furthermore, one coding gene subject to phasiRNA enrichment (*BLGH_05762*) encoded a putative secreted protein, and another (*BLGH_00843*) encoded a protein of unknown function. In total, 19 phasing loci were in the intergenic space. The majority of phasiRNAs were found in retrotransposons of *B. hordei*, that is, 42 *Tad*, 7 *HaTad*, 23 *Copia*, 29 *Gypsy*, and 23 *NonLTR* retrotransposons (Table S14), accounting for 124 loci altogether. One DNA transposon type *Mariner-2* and one unknown transposon were found as well. The most sensitive detection method with our data was unitas (Gebert et al., 2017), which predicted 1694 unique phasing loci in the genome of *B. hordei* (Table S14). These loci were randomly distributed on the scaffolds of *B. hordei* (Figure 6a). Of these, 135 were located in coding genes and 1535 in transposable elements, while 24 loci were intergenic (Figure 6c). Of the coding genes, 67 encoded Sgk2 kinases, while

seven encoded predicted secreted effector proteins. GO terms related to protein phosphorylation and organonitrogen metabolism were enriched in this set of genes (Figure 6d). The abundance of phasiRNAs in the different sites varied greatly; for example, the reads mapping to the Sgk2 kinase locus *BLGH_03674* were abundant in the MYC and EPI samples, while they were much less numerous in HAU and P40. Surprisingly, they were also very abundant in the EV+ fraction (Figure S13). Notably, there was no overlap regarding the phasiRNAs predicted by the three methods (Figure 6e).

3 | DISCUSSION

In this work, we sought to characterize the spectrum of sRNAs present in the context of a compatible barley–powdery mildew interaction by isolating and sequencing sRNAs from different "sites" of infected leaves: the epiphytic fungal structures that include the mycelium, runner hyphae, conidiophores, and conidia (MYC), the infected barley epidermis including plant tissue and the intracellular fungal haustoria (EPI), a fraction enriched in fungal haustoria (HAU), microsomes obtained after lysis of the epidermal cells (P40), and EVs from the apoplast of noninfected (EV−) and infected (EV+) leaves.

The first aim was to determine whether the sRNAs differed between the sites. First, we discovered abundant and highly specific fragments derived from 5.8S and 28S rRNA of barley and *B. hordei* and from tRNAs from *B. hordei* (rRFs and tRFs, respectively; Figure 2, Table 2). In most cases, these fragments were of discrete lengths (31–33 bases); they were derived from the 3′ end of the 5.8S rRNA or from specific locations within the 28S rRNA or they represented tRNA halves. The fragments exhibited highly specific and prominent

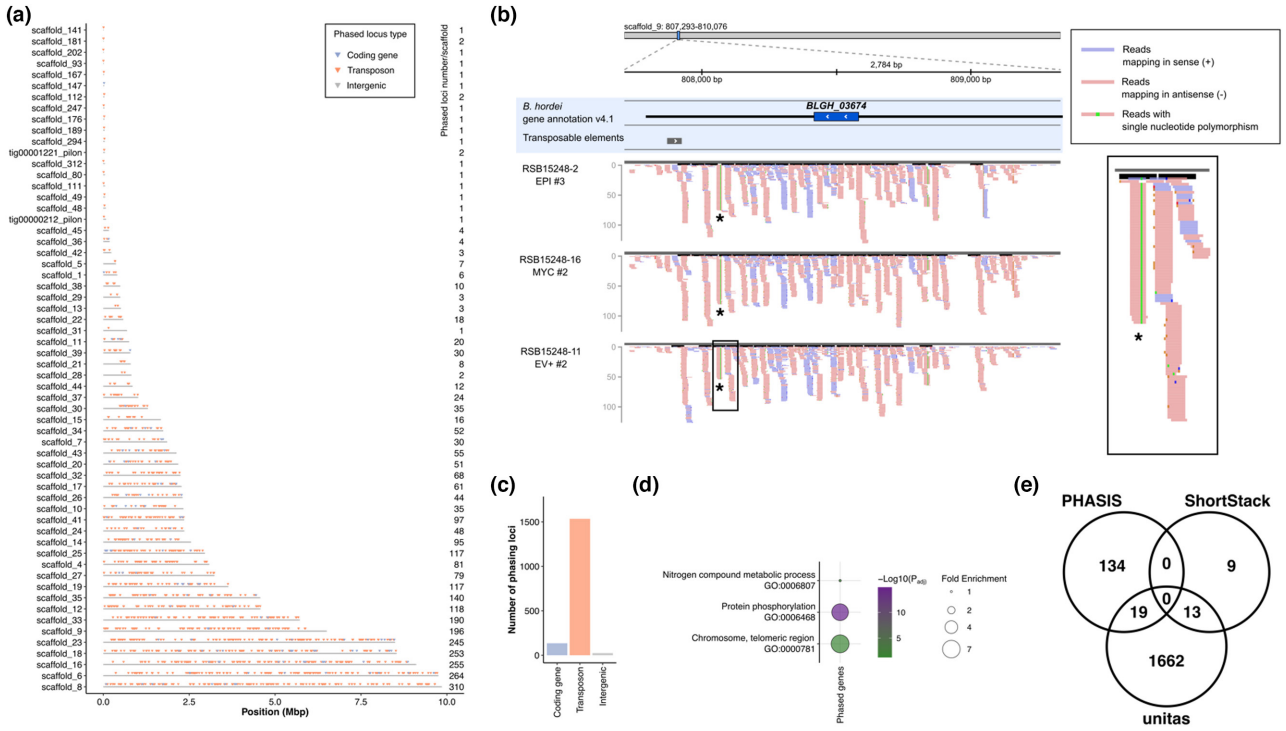

FIGURE 6 Transposable elements and genes encoding Sgk2 kinases are subject to phasing in *Blumeria hordei*. We identified phasiRNA-rich loci indicative of phasing in the genome of *B. hordei* with ShortStack pipeline v. 3.8.5-1 (Johnson et al., 2016), the PHASIS pipeline (Kakrana et al., 2017), and unitas v. 1.7.0 (Gebert et al., 2017). (a) Global distribution of predicted phasing loci in the genome of *B. hordei* DH14 (Frantzeskakis et al., 2018). The *x*-axis shows the genome position in Mb and the scaffolds are indicated on the *y*-axis. Triangles denote loci in which phasiRNAs were found with unitas. Blue triangles, phasing loci coinciding with annotated coding genes; orange triangles, phasing loci coinciding with transposable elements; grey triangles, intergenic phasing loci. (b) Example of one phased locus in *B. hordei*, containing the gene *BLGH_03674*, the partial open reading frame of a gene encoding a Sgk2 kinase. A subset of representative samples from sites where phasing in this locus was detected is shown (EPI, MYC, and EV+); the full set of samples is displayed in Figure S13. From top to bottom, the position on the scaffold, scaffold name and window, gene and transposable element annotations, and sample names are indicated. Red lines indicate reads mapping in sense orientation of the displayed sequence window; blue lines show reads mapping in antisense orientation. A zoom-in is shown on the right. The putative *trans*-acting small interfering RNA (tasiRNA) is indicated with an asterisk. The figure was generated after inspection with Integrative Genome Viewer (IGV; Robinson et al., 2017). (c) Bar graph summarizing the number of phasing loci types. The *x*-axis indicates the locus type, that is, coding gene, transposon, or intergenic; the *y*-axis shows the number of loci. (d) Gene ontology (GO) enrichment of phased coding genes was calculated with ShinyGO v. 0.75 (Ge et al., 2020); terms were summarized to nonredundant GO terms with EMBL-EBI QuickGO (https://www.ebi.ac.uk/QuickGO/) on GO v. 2022-04-26 and REVIGO (Supek et al., 2011). Bubble size indicates fold enrichment of the term in the respective subset, fill colour indicates $-\log_{10}$(FDR-adjusted enrichment *p* value). (e) Venn diagram summarizing the overlap of discovered phasing loci with the three methods.

enrichment at specific sites of the interaction; thus, they are unlikely to be the product of random RNA exonuclease degradation. Noncoding RNAs including tRNAs and rRNAs preferentially give rise to terminal fragments in animals (Chen et al., 2017; Li et al., 2012), fungi (Lee et al., 2009), and plants (Asha & Soniya, 2017). rRFs are involved in ageing in *Drosophila melanogaster* (Guan & Grigoriev, 2020), rRNA degradation in response to erroneous rRNA synthesis and UV irradiation stress in *Caenorhabditis elegans* (Zhou et al., 2017; Zhu et al., 2018), and the response to pathogen infection in black pepper (*Piper nigrum*; Asha & Soniya, 2017). The barley 5.8S-derived rRFs were abundant in both EV+ and EV− samples (Figure S10), suggesting their biogenesis is independent of the fungal infection in barley. By contrast, the barley 28S-derived rRFs could be induced by *B. hordei* infection, as they accumulated notably only in infected samples (HAU, P40, Figure S4). *B. hordei* 5.8S rRNA-derived rRFs were particularly abundant in isolated haustoria as well, suggestive of a role related to the intimate interaction with the host plant.

tRFs appear to be involved in multiple regulatory processes in plants (Alves & Nogueira, 2021). They may play a role in translation inhibition, because 5′-terminal oligoguanine-containing tRF halves of *A. thaliana* can inhibit translation in vitro (Lalande et al., 2020). They accumulate under various stresses, including phosphate starvation in barley and *A. thaliana* (Hackenberg et al., 2013; Hsieh et al., 2009) and *Fusarium graminearum* infection in wheat (Sun et al., 2022). Further, tRNA halves and 10–16-base tiny tRFs represent substantial portions of the sRNA pool in *A. thaliana* and may not be random tRNA degradation products (Ma et al., 2021). We observed fungal rather than plant tRFs of 31–32 bases specifically in isolated mycelium (Table 2). Some 28–35-base tRFs are abundant in appressoria of the rice blast pathogen *Magnaporthe oryzae* (Nunes et al., 2011), suggesting infection stage- or tissue-specific roles for these fragments in plant-pathogenic fungi. Intriguingly, the nitrogen-fixing bacterium *Bradyrhizobium japonicum* exchanges specific tRFs with its host plant soybean, hijacking the host RNAi machinery and supporting nodulation (Ren et al., 2019). While our data do not demonstrate *B. hordei* 31–32-base tRF exchange with the host, we detected tRFs in both infected epidermis and two EV+ samples (Figures 2 and S10), which hints at some tRFs occurring in vesicles and infected host cells.

An important question is how such rRFs and tRFs arise and how they are specifically enriched in plants and fungi. Both rRFs and tRFs can be generated by Dicer and loaded onto Ago. For example, 18–26-base tRFs accumulate in a DCL1-dependent manner and mediate Ago-driven cleavage of retrotransposons in *A. thaliana* (Martinez et al., 2017), and 23-base rRFs derived from the 5′ end of 5.8S rRNA are associated with AGO1 in *P. nigrum* (Asha & Soniya, 2017). In the fungus *Neurospora crassa*, the production of rRFs requires the RNA-dependent RNA polymerase QDE-1, the helicase QDE-3, and Dcl (Lee et al., 2009). However, the fragments we observed were longer than 26 nucleotides. Thus, they are unlikely to be associated with Dicer and Ago proteins. Instead, these specific tRFs and rRFs may have been generated by specific RNases, like the RNase A angiogenin in humans (Yamasaki et al., 2009), the *Saccharomyces cerevisiae* RNase T2 Rny1p (Thompson & Parker, 2009), and plant RNase T2 (Alves et al., 2017; Megel et al., 2019; Singh et al., 2020; Sun et al., 2022). RNase T2 most likely recognizes and hydrolyses single-stranded rRNA/tRNA loops, which could explain why the ends of the tRFs and rRFs we observed are always found in single-stranded loops (Figure 2). However, it is not clear why specific rRFs and tRFs accumulate while the remaining rRNA and tRNA molecules disappear. We found that these fragments potentially form novel secondary structures, which may render them inaccessible to RNA exonucleases, and that the barley 5.8S rRF may be energetically more stable than other fragments derived from the same molecule (Figure S6). However, this is not the case for all rRFs and tRFs we detected, suggesting that predicted thermodynamic stability alone cannot explain their high abundance. Future research will show if plants and pathogens repurposed specific fragments of these evolutionary ancient rRNA and tRNA molecules specifically towards intra- or cross-species communication.

Next, we turned our attention to miRNAs and milRNAs; in particular, we attempted to predict possible targets for endogenous and putative cross-kingdom gene regulation by RNAi. Cross-kingdom RNAi has been demonstrated to occur in interactions of plants with filamentous pathogens (Qiao et al., 2021), although its biological relevance at early stages of *A. thaliana* infection by *B. cinerea* is still under debate (He et al., 2023; Qin et al., 2023). We found that barley milRNAs are predicted to target more endogenous genes than fungal genes (Figures 5 and S11), while *B. hordei* milRNAs are predicted to target more genes cross-kingdom in barley. This trend was particularly evident in haustoria (76 of 108 milRNAs had calculated cross-kingdom targets). The process most frequently associated with putative gene targets for *H. vulgare* milRNAs in samples derived from epiphytic mycelium and infected epidermis is protein phosphorylation. Protein phosphorylation is important for signal transduction, for instance during plant defence (Park et al., 2012). Kinases have been reported as sRNA targets before. For example, *B. cinerea* sRNAs target *A. thaliana* mitogen-activated protein kinases and cell wall-associated kinases (Weiberg et al., 2013). Similarly, sRNAs from the wheat stripe rust *Puccinia striiformis* f. sp. *tritici* are predicted to target many kinase genes in wheat (Mueth et al., 2015), and *Fusarium oxysporum mil-R1* interferes with kinases of its host, tomato (Ji et al., 2021). A potential target could be the abundant Sgk2 kinases in *B. hordei* whose functions are unknown (Kusch et al., 2014), but for some of which we detected accumulation of phasiRNAs (Figure 6). Although fewer, there are also potential cross-kingdom targets for *B. hordei* milRNAs. For example, *B. hordei* milRNAs were predicted to target barley genes related to microtubule-severing ATPase activity, ADP binding, and nucleoside triphosphatase activity (Figure 5). Microtubules play key roles in cell growth and intercellular signalling, and the severing ATPase activity is essential for microtubule organization (Brandizzi & Wasteneys, 2013; Roll-Mecak & McNally, 2010). Interestingly, the bacterial effector HopZ1 destabilizes host plant microtubules and interferes with plant secretion (Lee et al., 2012). Therefore, it is possible that *B. hordei* miRNAs have evolved to interfere with microtubule dynamics in the host plant. However, contrary to cross-kingdom milRNAs from pathogens such as *B. cinerea* and *H.*

arabidopsidis, which appear to target host genes associated with plant immunity (Dunker et al., 2020; Weiberg et al., 2013), we did not find genes associated with the plant immune system over-represented in *B. hordei* milRNA cross-kingdom target genes in barley.

Remarkably, we also detected *B. hordei* milRNAs in EV+ samples. These milRNAs are unlikely to be contaminations because a considerable number (26 in total) of *B. hordei* milRNAs were specifically enriched in this sample type (Figure 4b). In principle, these EV+-enriched *B. hordei* milRNAs could originate from *B. hordei*-derived microsomes. However, the apoplastic space is physically separated from the main plant–fungus interaction site (the interface between the extrahaustorial membrane and the plant cell wall) by the haustorial neck band (Micali et al., 2011), which makes diffusion of vesicles of fungal origin into the apoplast unlikely. In principle, broken cells or breaking of cells or the haustorial neck during sample preparation are another possibility for the origin of these EVs. Also, during the vacuum infiltration process to obtain the apoplastic fluid, *B. hordei* EVs could be washed off the leaf surface and the mycelium. However, there was limited coenrichment of milRNAs in MYC and EV+ samples (Figure 4), and the EV+-specific milRNAs preclude this scenario. Therefore, it is possible that *B. hordei* milRNAs hijack barley EVs in a similar manner as turnip mosaic virus does in *Nicotiana benthamiana* (Movahed et al., 2019). The virus uses this mechanism to disperse its genetic material. Notably, this scenario would require the transition of fungal sRNAs through several stages of endo- and exocytosis.

PhasiRNAs have been well documented in plants, where they are thought to be the result of complex processes of controlled degradation of double-stranded RNAs; they play roles in a wide variety of biological processes, including development and plant immunity (Hou et al., 2019; Liu et al., 2020). Conversely, there is only very limited information about phasiRNA in fungi: To the best of our knowledge, the only case where phasiRNAs have been reported in the fungal kingdom is *Sclerotinia sclerotiorum* infected by a hypovirus (Lee Marzano et al., 2018). Therefore, we were surprised to find a clear signature of phasiRNA mapping to the fungal genome in *B. hordei* using ShortStack (Figure 6). We subsequently succeeded in detecting phasiRNAs using two other independent algorithms (unitas and PHASIS; Figure 6). The different pipelines detected somewhat different sets of phased loci in the *B. hordei* genome, which probably reflects the different mapping protocols. PHASIS exhibited the lowest overlap in phasing locations between the three tools; this is probably because PHASIS does not use already existing mapping files but performs its own mapping procedure instead. In any case, the low degree of overlap highlights the suboptimal performance of these tools for the identification of phasiRNA in filamentous fungi, and improvements may need to be implemented to determine complete phasiRNA complements in these organisms. The vast majority of phasiRNAs mapped to repetitive elements in the *B. hordei* genome, that is, transposons and the previously described abundant *Sgk2* kinase loci (Kusch et al., 2014). This may result from the involvement of phasiRNAs in controlling the expression of such genomic elements in the absence of the otherwise highly conserved repeat-induced point mutation (RIP) pathway (Frantzeskakis et al., 2018; Spanu et al., 2010). In animals, it is thought that PIWI-associated RNAs (which show analogous phasing to plant phasiRNAs) also function to control transposons in *Drosophila* (Kotov et al., 2019). Nevertheless, according to our data, some protein-coding gene loci in *B. hordei* show the presence of phased sRNAs as well, raising the possibility that the expression of these genes may be subject to regulation by RNAi.

The presence of predicted phasiRNAs of fungal origin in EVs of the leaf apoplast from infected barley leaves (EV+) is intriguing. It is difficult to rationalize what function, if any, these may have in modulating plant gene expression at remote sites. However, we note that *RNA3a* tasiRNAs derived from the *A. thaliana TAS3a* locus and synthesized within 3 h of pathogen infection may be an early mobile signal in systemic acquired resistance (Shine et al., 2022). Thus, it is conceivable that trafficking of sRNAs of fungal origin may follow the same route and may target plant gene expression (Hunt et al., 2019) and that fungal phasiRNAs in plant EVs are simply unintended by-products of this track. Overall, our findings further support the notion that phasing occurs in the fungal kingdom and additionally provide evidence that transposable elements in *B. hordei* are subject to sRNA-directed posttranscriptional regulation.

4 | EXPERIMENTAL PROCEDURES

4.1 | Plant cultivation

Barley (*H. vulgare* 'Margret') plants were grown in SoMi513 soil (Hawita) under a long day cycle (16 h light at 23°C, 8 h darkness at 20°C) at 60%–65% relative humidity and a light intensity of 105–120 $\mu mol\, s^{-1}\, m^{-2}$. Seven-day-old barley plants were inoculated with *B. hordei* strain K1; the plants were transferred to growth chambers with a long day cycle (12 h light at 20°C, 12 h dark at 19°C) at approximately 60% relative humidity and a light intensity of 100 $\mu mol\, s^{-1}\, m^{-2}$.

4.2 | Isolation of sRNAs

Seven-day-old barley was inoculated with *B. hordei* strain K1. At 4 days after inoculation, the primary leaves were harvested to isolate mycelia, epiphytic, haustoria, and microsomes from infected epidermis (P40). The dissection of the tissues and fractions was carried out as previously described (Li et al., 2019). Briefly, this consisted of dipping the excised leaves in cellulose acetate (5% wt/vol in acetone), letting the acetone evaporate for a few minutes, peeling first the epiphytic structures (MYC; this contained epiphytic mycelia, conidia, and spores), and then dissecting the adaxial barley epidermis (EPI).

A portion of the epidermis samples were subsequently used to extract haustoria (HAU) and epidermis microsomes (P40). First, the

plant cell walls were digested by incubating the epidermis in Onozuka R-10 cellulase (YAKULT pharmaceutical - Duchefa Biochemie BV; 2% wt/vol dissolved in potassium vesicle isolation buffer; 20 mM MES, 2 mM $CaCl_2$, 0.1 M KCl, pH 6.0; Rutter & Innes, 2017) for 2 h at 28°C on a rotary shaker (80 rpm). The digested epidermis samples were then filtered through a 40-µm nylon mesh sieve and centrifuged for 20 min at 200 × *g*. The pellet containing the haustoria was resuspended in 260 µL potassium vesicle isolation buffer and stored at −80°C (HAU); 1–2 × 10^6 haustoria were obtained per sample. The supernatant was centrifuged again at 10,000 × *g* for 30 min at 4°C, and the pellet was discarded. The resulting supernatant was centrifuged one last time at 40,000 × *g* at 4°C for 1 h; the pellet containing the microsomes was stored at −80°C (P40).

Apoplastic wash fluid was extracted from barley plants at 3 days after inoculation with *B. hordei* strain K1. Trays of both inoculated and noninoculated plants were covered with lids and incubated prior to apoplastic wash fluid extraction. Approximately 30 g of leaf fresh weight was collected and vacuum-infiltrated with potassium vesicle isolation buffer. Excess buffer was carefully removed and the leaves were placed with the cut ends down in 20-mL syringes. The syringes were inserted into 50-mL centrifuge tubes. Apoplastic wash fluid was collected at 400 × *g* for 12 min at 4°C. Cellular debris was first removed by passing the apoplastic wash fluid through a 0.22-µm syringe filter and further by centrifugation at 10,000 × *g* for 30 min at 4°C. A crude EV fraction was isolated from apoplastic wash fluid based on a protocol by (Rutter & Innes, 2017). The apoplastic wash fluid was centrifuged for 1 h at 40,000 × *g* (4°C) in a swinging bucket rotor to collect EVs (EV− and EV+). The crude EV pellet was resuspended in 50 µL 20 mM Tris–HCl (pH 7.5) and not further purified.

The MYC and EPI samples were ground in liquid nitrogen with quartz sand in a chilled pestle and mortar and RNA was extracted from all samples using TRIzol (Thermo Scientific) as described by the manufacturer. The RNA from all other samples was extracted by resuspending the frozen samples directly into TRIzol reagent and proceeding as described. The quantity and quality of the RNA were determined by spectrophotometry (NanoDrop; Thermo Scientific) and spectrofluorimetry (Qubit; Thermo Scientific).

4.3 | sRNA sequencing and data processing

RNA samples were quantified via the Qubit RNA HS Assay (Thermo Scientific) and sized with a High Sensitivity RNA ScreenTape (Agilent). Library preparation was performed with RealSeq-Dual as recommended by the manufacturer (RealSeq Biosciences; Barberán-Soler et al., 2018) with 100 ng of RNA for each sample. Half the volume of each library was amplified by 20 cycles of PCR. Libraries from all samples were pooled for sequencing in the same flow cell of a NextSeq single-end 75-nucleotide reads run. FastQ files were trimmed of adapter sequences using Cutadapt (Martin, 2011) with the following parameters: cutadapt -u 1 -a TGGAATTCTCGGGTGCCAAGG -m 15. We further performed quality trimming of reads with Trimmomatic v. 0.39 (Bolger et al., 2014). FASTQ read data were inspected using FastQC v. 0.11.5 (Babraham Bioinformatics). FASTQ/FASTA files were parsed with SeqKit v. 2.1.0 (Shen et al., 2016).

4.4 | Read length distribution analysis

We determined read length counts with custom BASH scripts and plotted these data using ggplot2 v. 3.3.4 (Wickham, 2009) in R v. 4.1.2 (R Core Team, 2021). Reads were mapped to the reference genomes of *H. vulgare* (Hordeum_vulgare.IBSC_v2; Mascher et al., 2017) and *B. hordei* DH14 v4 (Frantzeskakis et al., 2018) using bowtie within the ShortStack pipeline v. 3.8.5-1 (Johnson et al., 2016). We used SAMtools v. 1.9 (Li et al., 2009) in conjunction with custom BASH scripts to parse read mapping statistics. Read counts by genomic features, that is, coding genes, transposable elements, and milRNA genes identified by ShortStack, were determined using featureCounts v. 2.0.1 (Liao et al., 2014). *H. vulgare* transposable elements were identified with RepeatMasker v. 4.0.7 (http://www.repeatmasker.org) using the repeat database version RepBase-20170127 and "-species Hordeum". The data were plotted with ggplot2 v. 3.3.4 (Wickham, 2009) in R v. 4.1.2 (R Core Team, 2021).

4.5 | Read BLAST searches

We used a custom Python script to generate FASTA files containing reads of 21–22 bases, 31–32 bases, and 32–33 bases, respectively, and then deduplicated reads using clumpify.sh of the BBmap package (https://jgi.doe.gov/data-and-tools/software-tools/bbtools/). We downloaded the rRNA and tRNA molecules deposited in the RFAM database (http://ftp.ebi.ac.uk/pub/databases/Rfam/CURRENT/fasta_files/) in October 2021. All reads were aligned to the RFAM databases using MMSeqs2 v9.d36de (Steinegger & Söding, 2017). Reads aligning to RF02543 (28S rRNA) were subsequently aligned to the 28S rRNA sequences of *H. vulgare* (RNAcentral accession URS0002132C2A_4513) and *B. hordei* (URS0002174482_62688). Read alignment coverage was determined via BEDtools v. 2.25.0 (Quinlan & Hall, 2010). Bar graphs and histograms displaying these data were plotted with ggplot2 v. 3.3.4 (Wickham, 2009) in R v. 4.1.2 (R Core Team, 2021).

4.6 | Structure and free energy analysis of rRNA and tRNA fragments

We obtained rRNA and tRNA structures predicted by R2DT from RNAcentral (https://rnacentral.org) and visualized the structures with Forna (Kerpedjiev et al., 2015). We further used the Vienna RNAfold v. 2.4.18 web server (Gruber et al., 2008) to calculate

secondary structures of 5.8S rRNAs, rRFs, and tRFs and their MFE values.

4.7 | Identification of milRNAs

We used ShortStack pipeline v. 3.8.5-1 (Johnson et al., 2016) to predict milRNAs in the genomes of *H. vulgare* (Hordeum_vulgare. IBSC_v2; Mascher et al., 2017) and *B. hordei* DH14 (Frantzeskakis et al., 2018). sRNAs with a Dicer Call cut-off of N15 were considered as milRNAs. We collected nonredundant *B. hordei* and *H. vulgare* miRNAs and milRNAs in GFF and FASTA formats in Files S2–S5. featureCounts v2.0.1 (Liao et al., 2014) was used to determine milRNA locus-specific read counts.

4.8 | Quantification and clustering of milRNA expression

We first analysed similarities/differences between samples using several statistical approaches. NMDS collapses multidimensional information into fewer dimensions and does not require a normal distribution. The stress value represented the statistical fit of the model for the data. Stress values equal to or below 0.05 indicated a good model fit. We complemented the NMDS analysis with metric multidimensional scaling (MDS), PCA, and Pearson coefficient correlation (PCC)-based hierarchical clustering. In addition, nonparametric rank-based ANOSIM tests were performed to determine statistical differences between samples.

WGCNA (Langfelder & Horvath, 2008) was performed using read counts mapping to milRNA loci. First, we filtered out the nonexpressed genes (cut-off TPM < 1), leaving 22,415 *H. vulgare* and 2217 *B. hordei* milRNAs for the construction of the coexpression networks. The scale-free network distribution required determination of the soft threshold β (12 for *H. vulgare* and 16 for *B. hordei*) of the adjacency matrix. A module correlation of 0.1 with either sample was the cut-off for identifying milRNAs enriched in the samples MYC, EPI, HAU, P40, and EV+; we then refined assignment of milRNAs to samples at >2.5-fold above average expression across samples. We used pairwise differential expression analysis with DESeq2 (Love et al., 2014), EdgeR (Robinson et al., 2010), and limma-VOOM (Law et al., 2014) to confirm the overall expression trends of milRNAs from *H. vulgare* and *B. hordei*. Intersections were analysed by UpSetR plots using ComplexUpset (Lex et al., 2014).

4.9 | sRNA target prediction and GO enrichment of milRNA target sets

We used psRNAtarget (https://www.zhaolab.org/psRNATarget) Schema V2 2017 release (Dai & Zhao, 2011) at an expectation value cut-off of 2. We performed GO enrichment analysis on putative milRNA target gene sets using ShinyGO v. 0.75 (Ge et al., 2020); *p* values indicated were calculated via false discovery rate (FDR) correction (p_{adj}). GO terms were summarized by removing redundant GO terms with EMBL-EBI QuickGO (https://www.ebi.ac.uk/QuickGO/) in GO v. 2022-04-26 and REVIGO (Supek et al., 2011) with the Gene Ontology database and the UniProt-to-GO mapping database from the EBI GOA project (versions from November 2021).

4.10 | PhasiRNA and tasiRNA detection in *B. hordei*

We used ShortStack pipeline v. 3.8.5-1 (Johnson et al., 2016), the PHASIS pipeline (Kakrana et al., 2017), unitas v. 1.7.0 (Gebert et al., 2017), and PhaseTank v. 1.0 (Guo et al., 2015) to detect evidence of phasing in the genome of *B. hordei* with our sRNA-seq dataset. Detected phasing sites were concatenated to nonredundant phasing loci using BEDtools v. 2.25.0 (Quinlan & Hall, 2010). Manual inspection of phasing loci was done using Integrative Genomics Viewer (Robinson et al., 2017).

ACKNOWLEDGEMENTS

We thank Blake Meyers for advice on the usage of PHASIS and members of the Deutsche Forschungsgemeinschaft (DFG, German Research Foundation)-funded FOR5116 consortium for critical feedback. The analysis was performed with computing resources granted by RWTH Aachen University under project ID rwth0146.

FUNDING INFORMATION

P.D.S. was funded by a research fellowship from the Leverhulme Trust (RF-2019-053), a research award by the Alexander von Humboldt Foundation (GBR 1204122 GSA), and a Theodore von Kármán Fellowship (RWTH Aachen). H.T. was supported by the RWTH Aachen scholarship for doctoral students. The work was further supported by DFG project number 433194101 (grant PA 861/22-1 to R.P.) in the context of the Research Unit consortium FOR5116 "exRNA" and project number 274444799 (grant 861/14-2 awarded to R.P.) in the context of the DFG-funded Priority Program SPP1819 "Rapid evolutionary adaptation – potential and constraints."

DATA AVAILABILITY STATEMENT

The sRNA sequencing data are deposited at NCBI at www.ncbi.nlm.nih.gov/bioproject/ as accession PRJNA809109; the SRA accessions are listed in Table S1. The *B. hordei* and *H. vulgare* miRNAs and milRNAs are available in GFF format and FASTA format in Files S2–S5. Custom codes for our analysis pipeline are available at https://github.com/stefankusch/smallRNA_seq_analysis.

ORCID

Stefan Kusch https://orcid.org/0000-0002-2472-5255
Hannah Thieron https://orcid.org/0000-0002-0670-7328
Pietro D. Spanu https://orcid.org/0000-0001-8928-6049
Ralph Panstruga https://orcid.org/0000-0002-3756-8957

REFERENCES

Alves, C.S. & Nogueira, F.T.S. (2021) Plant small RNA world growing bigger: tRNA-derived fragments, longstanding players in regulatory processes. *Frontiers in Molecular Biosciences*, 8, 638911.

Alves, C.S., Vicentini, R., Duarte, G.T., Pinoti, V.F., Vincentz, M. & Nogueira, F.T.S. (2017) Genome-wide identification and characterization of tRNA-derived RNA fragments in land plants. *Plant Molecular Biology*, 93, 35–48.

An, Q.L., Ehlers, K., Kogel, K.H., van Bel, A.J.E. & Hückelhoven, R. (2006) Multivesicular compartments proliferate in susceptible and resistant MLA12-barley leaves in response to infection by the biotrophic powdery mildew fungus. *The New Phytologist*, 172, 563–576.

Asha, S. & Soniya, E.V. (2017) The sRNAome mining revealed existence of unique signature small RNAs derived from 5.8SrRNA from *Piper nigrum* and other plant lineages. *Scientific Reports*, 7, 41052.

Barberán-Soler, S., Vo, J.M., Hogans, R.E., Dallas, A., Johnston, B.H. & Kazakov, S.A. (2018) Decreasing miRNA sequencing bias using a single adapter and circularization approach. *Genome Biology*, 19, 105.

Bolger, A.M., Lohse, M. & Usadel, B. (2014) Trimmomatic: a flexible trimmer for Illumina sequence data. *Bioinformatics*, 30, 2114–2120.

Bologna, N.G. & Voinnet, O. (2014) The diversity, biogenesis, and activities of endogenous silencing small RNAs in *Arabidopsis*. *Annual Review of Plant Biology*, 65, 473–503.

Brandizzi, F. & Wasteneys, G.O. (2013) Cytoskeleton-dependent endomembrane organization in plant cells: an emerging role for microtubules. *The Plant Journal*, 75, 339–349.

Cai, Q., Qiao, L., Wang, M., He, B., Lin, F.-M., Palmquist, J. et al. (2018) Plants send small RNAs in extracellular vesicles to fungal pathogen to silence virulence genes. *Science*, 360, 1126–1129.

Chen, X. & Rechavi, O. (2022) Plant and animal small RNA communications between cells and organisms. *Nature Reviews Molecular Cell Biology*, 23, 185–203.

Chen, Z., Sun, Y., Yang, X., Wu, Z., Guo, K., Niu, X. et al. (2017) Two featured series of rRNA-derived RNA fragments (rRFs) constitute a novel class of small RNAs. *PLoS One*, 12, e0176458.

Dai, X. & Zhao, P.X. (2011) psRNATarget: a plant small RNA target analysis server. *Nucleic Acids Research*, 39, W155–W159.

Deng, P., Wang, L., Cui, L., Feng, K., Liu, F., Du, X. et al. (2015) Global identification of microRNAs and their targets in barley under salinity stress. *PLoS One*, 10, e0137990.

Derbyshire, M., Mbengue, M., Barascud, M., Navaud, O. & Raffaele, S. (2019) Small RNAs from the plant pathogenic fungus *Sclerotinia sclerotiorum* highlight host candidate genes associated with quantitative disease resistance. *Molecular Plant Pathology*, 20, 1279–1297.

Dunker, F., Trutzenberg, A., Rothenpieler, J.S., Kuhn, S., Pröls, R., Schreiber, T. et al. (2020) Oomycete small RNAs bind to the plant RNA-induced silencing complex for virulence. *eLife*, 9, e56096.

Fire, A., Xu, S., Montgomery, M.K., Kostas, S.A., Driver, S.E. & Mello, C.C. (1998) Potent and specific genetic interference by double-stranded RNA in *Caenorhabditis elegans*. *Nature*, 391, 806–811.

Frantzeskakis, L., Kracher, B., Kusch, S., Yoshikawa-Maekawa, M., Bauer, S., Pedersen, C. et al. (2018) Signatures of host specialization and a recent transposable element burst in the dynamic one-speed genome of the fungal barley powdery mildew pathogen. *BMC Genomics*, 19, 27.

Fukudome, A. & Fukuhara, T. (2017) Plant Dicer-like proteins: double-stranded RNA-cleaving enzymes for small RNA biogenesis. *Journal of Plant Research*, 130, 33–44.

Ge, S.X., Jung, D. & Yao, R. (2020) ShinyGO: a graphical gene-set enrichment tool for animals and plants. *Bioinformatics*, 36, 2628–2629.

Gebert, D., Hewel, C. & Rosenkranz, D. (2017) Unitas: the universal tool for annotation of small RNAs. *BMC Genomics*, 18, 644.

Gruber, A.R., Lorenz, R., Bernhart, S.H., Neuböck, R. & Hofacker, I.L. (2008) The Vienna RNA websuite. *Nucleic Acids Research*, 36, W70–W74.

Guan, L. & Grigoriev, A. (2020) Age-related Argonaute loading of ribosomal RNA fragments. *MicroRNA*, 9, 142–152.

Guo, Q., Qu, X. & Jin, W. (2015) PhaseTank: genome-wide computational identification of phasiRNAs and their regulatory cascades. *Bioinformatics*, 31, 284–286.

Hackenberg, M., Huang, P.-J., Huang, C.-Y., Shi, B.-J., Gustafson, P. & Langridge, P. (2013) A comprehensive expression profile of microRNAs and other classes of non-coding small RNAs in barley under phosphorous-deficient and -sufficient conditions. *DNA Research*, 20, 109–125.

He, B., Cai, Q., Weiberg, A., Li, W., Cheng, A.-P., Ouyang, S. et al. (2023) *Botrytis cinerea* small RNAs are associated with tomato AGO1 and silence tomato defense-related target genes supporting cross-kingdom RNAi. *bioRxiv*. DOI:10.1101/2022.12.30.522274 [preprint].

He, B., Hamby, R. & Jin, H. (2021) Plant extracellular vesicles: Trojan horses of cross-kingdom warfare. *FASEB BioAdvances*, 3, 657–664.

Hippe, S. (1985) Ultrastructure of haustoria of *Erysiphe graminis* f. sp. *hordei* preserved by freeze-substitution. *Protoplasma*, 129, 52–61.

Hou, Y., Zhai, Y., Feng, L., Karimi, H.Z., Rutter, B.D., Zeng, L. et al. (2019) A *Phytophthora* effector suppresses trans-kingdom RNAi to promote disease susceptibility. *Cell Host & Microbe*, 25, 153–165.e5.

Hsieh, L.-C., Lin, S.-I., Shih, A.C.-C., Chen, J.-W., Lin, W.-Y., Tseng, C.-Y. et al. (2009) Uncovering small RNA-mediated responses to phosphate deficiency in *Arabidopsis* by deep sequencing. *Plant Physiology*, 151, 2120–2132.

Hunt, M., Banerjee, S., Surana, P., Liu, M., Fuerst, G., Mathioni, S. et al. (2019) Small RNA discovery in the interaction between barley and the powdery mildew pathogen. *BMC Genomics*, 20, 345.

Ji, H.-M., Mao, H.-Y., Li, S.-J., Feng, T., Zhang, Z.-Y., Cheng, L. et al. (2021) *Fol*-milR1, a pathogenicity factor of *Fusarium oxysporum*, confers tomato wilt disease resistance by impairing host immune responses. *The New Phytologist*, 232, 705–718.

Johnson, N.R., Yeoh, J.M., Coruh, C. & Axtell, M.J. (2016) Improved placement of multi-mapping small RNAs, *G3*, 6, 2103–2111.

Kakrana, A., Li, P., Patel, P., Hammond, R., Anand, D., Mathioni, S.M. et al. (2017) PHASIS: a computational suite for de novo discovery and characterization of phased, siRNA-generating loci and their miRNA triggers. *bioRxiv*. DOI: 10.1101/158832 [preprint].

Kerpedjiev, P., Hammer, S. & Hofacker, I.L. (2015) Forna (force-directed RNA): simple and effective online RNA secondary structure diagrams. *Bioinformatics*, 31, 3377–3379.

Klesen, S., Hill, K. & Timmermans, M.C.P. (2020) Small RNAs as plant morphogens. *Current Topics in Developmental Biology*, 137, 455–480.

Komiya, R. (2017) Biogenesis of diverse plant phasiRNAs involves an miRNA-trigger and Dicer-processing. *Journal of Plant Research*, 130, 17–23.

Kotov, A.A., Adashev, V.E., Godneeva, B.K., Ninova, M., Shatskikh, A.S., Bazylev, S.S. et al. (2019) piRNA silencing contributes to interspecies hybrid sterility and reproductive isolation in *Drosophila melanogaster*. *Nucleic Acids Research*, 47, 4255–4271.

Kusch, S., Ahmadinejad, N., Panstruga, R. & Kuhn, H. (2014) *In silico* analysis of the core signaling proteome from the barley powdery mildew pathogen (*Blumeria graminis* f.sp. *hordei*). *BMC Genomics*, 15, 843.

Kusch, S., Frantzeskakis, L., Thieron, H. & Panstruga, R. (2018) Small RNAs from cereal powdery mildew pathogens may target host plant genes. *Fungal Biology*, 122, 1050–1063.

Lalande, S., Merret, R., Salinas-Giegé, T. & Drouard, L. (2020) *Arabidopsis* tRNA-derived fragments as potential modulators of translation. *RNA Biology*, 17, 1137–1148.

Langfelder, P. & Horvath, S. (2008) WGCNA: an R package for weighted correlation network analysis. *BMC Bioinformatics*, 9, 559.

Law, C.W., Chen, Y., Shi, W. & Smyth, G.K. (2014) Voom: precision weights unlock linear model analysis tools for RNA-seq read counts. *Genome Biology*, 15, R29.

Lee, A.H.-Y., Hurley, B., Felsensteiner, C., Yea, C., Ckurshumova, W., Bartetzko, V. et al. (2012) A bacterial acetyltransferase destroys plant microtubule networks and blocks secretion. *PLoS Pathogens*, 8, e1002523.

Lee, H.-C., Chang, S.-S., Choudhary, S., Aalto, A.P., Maiti, M., Bamford, D.H. et al. (2009) qiRNA is a new type of small interfering RNA induced by DNA damage. *Nature*, 459, 274–277.

Lee, H.-C., Li, L., Gu, W., Xue, Z., Crosthwaite, S.K., Pertsemlidis, A. et al. (2010) Diverse pathways generate microRNA-like RNAs and Dicer-independent small interfering RNAs in fungi. *Molecular Cell*, 38, 803–814.

Lee Marzano, S.-Y., Neupane, A. & Domier, L. (2018) Transcriptional and small RNA responses of the white mold fungus *Sclerotinia sclerotiorum* to infection by a virulence-attenuating hypovirus. *Viruses*, 10, 713–728.

Lex, A., Gehlenborg, N., Strobelt, H., Vuillemot, R. & Pfister, H. (2014) UpSet: visualization of intersecting sets. *IEEE Transactions on Visualization and Computer Graphics*, 20, 1983–1992.

Li, H., Handsaker, B., Wysoker, A., Fennell, T., Ruan, J., Homer, N. et al. (2009) The sequence alignment/map format and SAMtools. *Bioinformatics*, 25, 2078–2079.

Li, L., Collier, B. & Spanu, P. (2019) Isolation of powdery mildew haustoria from infected barley. *Bio-Protocol*, 9, e3299.

Li, Z., Ender, C., Meister, G., Moore, P.S., Chang, Y. & John, B. (2012) Extensive terminal and asymmetric processing of small RNAs from rRNAs, snoRNAs, snRNAs, and tRNAs. *Nucleic Acids Research*, 40, 6787–6799.

Liao, Y., Smyth, G.K. & Shi, W. (2014) featureCounts: an efficient general purpose program for assigning sequence reads to genomic features. *Bioinformatics*, 30, 923–930.

Liu, M., Braun, U., Takamatsu, S., Hambleton, S., Shoukouhi, P., Bisson, K.R. et al. (2021) Taxonomic revision of *Blumeria* based on multi-gene DNA sequences, host preferences and morphology. *Mycoscience*, 62, 143–165.

Liu, Y., Teng, C., Xia, R. & Meyers, B.C. (2020) PhasiRNAs in plants: their biogenesis, genic sources, and roles in stress responses, development, and reproduction. *The Plant Cell*, 32, 3059–3080.

Love, M.I., Huber, W. & Anders, S. (2014) Moderated estimation of fold change and dispersion for RNA-seq data with DESeq2. *Genome Biology*, 15, 550.

Ma, X., Liu, C., Kong, X., Liu, J., Zhang, S., Liang, S. et al. (2021) Extensive profiling of the expressions of tRNAs and tRNA-derived fragments (tRFs) reveals the complexities of tRNA and tRF populations in plants. *Science China. Life Sciences*, 64, 495–511.

Ma, X., Wiedmer, J. & Palma-Guerrero, J. (2019) Small RNA bidirectional crosstalk during the interaction between wheat and *Zymoseptoria tritici*. *Frontiers in Plant Science*, 10, 1669.

Manocha, M.S. & Shaw, M. (1964) Occurrence of lomasomes in mesophyll cells of 'Khapli' wheat. *Nature*, 203, 1402–1403.

Martin, M. (2011) Cutadapt removes adapter sequences from high-throughput sequencing reads. *EMBnet Journal*, 17, 10.

Martinez, G., Choudury, S.G. & Slotkin, R.K. (2017) tRNA-derived small RNAs target transposable element transcripts. *Nucleic Acids Research*, 45, 5142–5152.

Mascher, M., Gundlach, H., Himmelbach, A., Beier, S., Twardziok, S.O., Wicker, T. et al. (2017) A chromosome conformation capture ordered sequence of the barley genome. *Nature*, 544, 427–433.

Megel, C., Hummel, G., Lalande, S., Ubrig, E., Cognat, V., Morelle, G. et al. (2019) Plant RNases T2, but not dicer-like proteins, are major players of tRNA-derived fragments biogenesis. *Nucleic Acids Research*, 47, 941–952.

Micali, C.O., Neumann, U., Grunewald, D., Panstruga, R. & O'Connell, R. (2011) Biogenesis of a specialized plant-fungal interface during host cell internalization of *Golovinomyces orontii* haustoria. *Cellular Microbiology*, 13, 210–226.

Morelli, A.E., Larregina, A.T., Shufesky, W.J., Sullivan, M.L.G., Stolz, D.B., Papworth, G.D. et al. (2004) Endocytosis, intracellular sorting, and processing of exosomes by dendritic cells. *Blood*, 104, 3257–3266.

Movahed, N., Cabanillas, D.G., Wan, J., Vali, H., Laliberté, J.-F. & Zheng, H. (2019) Turnip mosaic virus components are released into the extracellular space by vesicles in infected leaves. *Plant Physiology*, 180, 1375–1388.

Mueth, N.A., Ramachandran, S.R. & Hulbert, S.H. (2015) Small RNAs from the wheat stripe rust fungus (*Puccinia striiformis* f.sp. *tritici*). *BMC Genomics*, 16, 718.

Nunes, C.C., Gowda, M., Sailsbery, J., Xue, M., Chen, F., Brown, D.E. et al. (2011) Diverse and tissue-enriched small RNAs in the plant pathogenic fungus, *Magnaporthe oryzae*. *BMC Genomics*, 12, 288.

Park, C.-J., Caddell, D.F. & Ronald, P.C. (2012) Protein phosphorylation in plant immunity: insights into the regulation of pattern recognition receptor-mediated signaling. *Frontiers in Plant Science*, 3, 177.

Parolini, I., Federici, C., Raggi, C., Lugini, L., Palleschi, S., de Milito, A. et al. (2009) Microenvironmental pH is a key factor for exosome traffic in tumor cells. *The Journal of Biological Chemistry*, 284, 34211–34222.

Qiao, Y., Xia, R., Zhai, J., Hou, Y., Feng, L., Zhai, Y. et al. (2021) Small RNAs in plant immunity and virulence of filamentous pathogens. *Annual Review of Phytopathology*, 59, 265–288.

Qin, S., Veloso, J., Baak, M., Boogmans, B., Bosman, T., Puccetti, G. et al. (2023) Molecular characterization reveals no functional evidence for naturally occurring cross-kingdom RNA interference in the early stages of *Botrytis cinerea*-tomato interaction. *Molecular Plant Pathology*, 24, 3–15.

Quinlan, A.R. & Hall, I.M. (2010) BEDTools: a flexible suite of utilities for comparing genomic features. *Bioinformatics*, 26, 841–842.

R Core Team. (2021) R: a language and environment for statistical computing. http://www.R-project.org/ [Accessed 9th March 2023].

Ragupathy, R., Ravichandran, S., Mahdi, M.S.R., Huang, D., Reimer, E., Domaratzki, M. et al. (2016) Deep sequencing of wheat sRNA transcriptome reveals distinct temporal expression pattern of miRNAs in response to heat, light and UV. *Scientific Reports*, 6, 39373.

Ren, B., Wang, X., Duan, J. & Ma, J. (2019) Rhizobial tRNA-derived small RNAs are signal molecules regulating plant nodulation. *Science*, 365, 919–922.

Robinson, J.T., Thorvaldsdóttir, H., Wenger, A.M., Zehir, A. & Mesirov, J.P. (2017) Variant review with the integrative genomics viewer. *Cancer Research*, 77, e31–e34.

Robinson, M.D., McCarthy, D.J. & Smyth, G.K. (2010) edgeR: a Bioconductor package for differential expression analysis of digital gene expression data. *Bioinformatics*, 26, 139–140.

Roll-Mecak, A. & McNally, F.J. (2010) Microtubule-severing enzymes. *Current Opinion in Cell Biology*, 22, 96–103.

Rutter, B.D. & Innes, R.W. (2017) Extracellular vesicles isolated from the leaf apoplast carry stress-response proteins. *Plant Physiology*, 173, 728–741.

Segura, E., Guérin, C., Hogg, N., Amigorena, S. & Théry, C. (2007) $CD8^+$ dendritic cells use LFA-1 to capture MHC-peptide complexes from exosomes in vivo. *Journal of Immunology*, 179, 1489–1496.

Shen, W., Le, S., Li, Y. & Hu, F. (2016) SeqKit: a cross-platform and ultrafast toolkit for FASTA/Q file manipulation. *PLoS One*, 11, e0163962.

Shine, M.B., Zhang, K., Liu, H., Lim, G.-H., Xia, F., Yu, K. et al. (2022) Phased small RNA-mediated systemic signaling in plants. *Science Advances*, 8, eabm8791.

Singh, N.K., Paz, E., Kutsher, Y., Reuveni, M. & Lers, A. (2020) Tomato T2 ribonuclease LE is involved in the response to pathogens. *Molecular Plant Pathology*, 21, 895–906.

Skokos, D., Le Panse, S., Villa, I., Rousselle, J.C., Peronet, R., David, B. et al. (2001) Mast cell-dependent B and T lymphocyte activation

is mediated by the secretion of immunologically active exosomes. *Journal of Immunology*, 166, 868–876.

Spanu, P.D., Abbott, J.C., Amselem, J., Burgis, T.A., Soanes, D.M., Stüber, K. et al. (2010) Genome expansion and gene loss in powdery mildew fungi reveal tradeoffs in extreme parasitism. *Science*, 330, 1543–1546.

Steinegger, M. & Söding, J. (2017) MMseqs2 enables sensitive protein sequence searching for the analysis of massive data sets. *Nature Biotechnology*, 35, 1026–1028.

Sun, Z., Hu, Y., Zhou, Y., Jiang, N., Hu, S., Li, L. et al. (2022) tRNA-derived fragments from wheat are potentially involved in susceptibility to Fusarium head blight. *BMC Plant Biology*, 22, 3.

Supek, F., Bošnjak, M., Škunca, N. & Šmuc, T. (2011) REVIGO summarizes and visualizes long lists of gene ontology terms. *PLoS One*, 6, e21800.

Thompson, D.M. & Parker, R. (2009) The RNase Rny1p cleaves tRNAs and promotes cell death during oxidative stress in *Saccharomyces cerevisiae*. *The Journal of Cell Biology*, 185, 43–50.

Wang, M., Weiberg, A., Lin, F.-M., Thomma, B.P.H.J., Huang, H.-D. & Jin, H. (2016) Bidirectional cross-kingdom RNAi and fungal uptake of external RNAs confer plant protection. *Nature Plants*, 2, 16151.

Weiberg, A., Wang, M., Lin, F.-M., Zhao, H., Zhang, Z., Kaloshian, I. et al. (2013) Fungal small RNAs suppress plant immunity by hijacking host RNA interference pathways. *Science*, 342, 118–123.

Wickham, H. (2009) *ggplot2. Elegant graphics for data analysis*. New York: Springer.

Woith, E., Fuhrmann, G. & Melzig, M.F. (2019) Extracellular vesicles-connecting kingdoms. *International Journal of Molecular Sciences*, 20, 5695–5721.

Wong-Bajracharya, J., Singan, V.R., Monti, R., Plett, K.L., Ng, V., Grigoriev, I.V. et al. (2022) The ectomycorrhizal fungus *Pisolithus microcarpus* encodes a microRNA involved in cross-kingdom gene silencing during symbiosis. *Proceedings of the National Academy of Sciences of the United States of America*, 119, e2103527119.

Wu, L., Yu, J., Shen, Q., Huang, L., Wu, D. & Zhang, G. (2018) Identification of microRNAs in response to aluminum stress in the roots of Tibetan wild barley and cultivated barley. *BMC Genomics*, 19, 560.

Xin, M., Wang, Y., Yao, Y., Song, N., Hu, Z., Qin, D. et al. (2011) Identification and characterization of wheat long non-protein coding RNAs responsive to powdery mildew infection and heat stress by using microarray analysis and SBS sequencing. *BMC Plant Biology*, 11, 61.

Yamasaki, S., Ivanov, P., Hu, G.-F. & Anderson, P. (2009) Angiogenin cleaves tRNA and promotes stress-induced translational repression. *The Journal of Cell Biology*, 185, 35–42.

Zand Karimi, H., Baldrich, P., Rutter, B.D., Borniego, L., Zajt, K.K., Meyers, B.C. et al. (2022) *Arabidopsis* apoplastic fluid contains sRNA- and circular RNA–protein complexes that are located outside extracellular vesicles. *The Plant Cell*, 34, 1863–1881.

Zhang, T., Zhao, Y.-L., Zhao, J.-H., Wang, S., Jin, Y., Chen, Z.-Q. et al. (2016) Cotton plants export microRNAs to inhibit virulence gene expression in a fungal pathogen. *Nature Plants*, 2, 16153.

Zhou, X., Feng, X., Mao, H., Li, M., Xu, F., Hu, K. et al. (2017) RdRP-synthesized antisense ribosomal siRNAs silence pre-rRNA via the nuclear RNAi pathway. *Nature Structural & Molecular Biology*, 24, 258–269.

Zhu, C., Liu, J.-H., Zhao, J.-H., Liu, T., Chen, Y.-Y., Wang, C.-H. et al. (2022) A fungal effector suppresses the nuclear export of AGO1-miRNA complex to promote infection in plants. *Proceedings of National Academy of Sciences United States of America*, 119, e2114583119.

Zhu, C., Yan, Q., Weng, C., Hou, X., Mao, H., Liu, D. et al. (2018) Erroneous ribosomal RNAs promote the generation of antisense ribosomal siRNA. *Proceedings of National Academy of Sciences United States of America*, 115, 10082–10087.

SUPPORTING INFORMATION

Additional supporting information can be found online in the Supporting Information section at the end of this article.

How to cite this article: Kusch, S., Singh, M., Thieron, H., Spanu, P.D. & Panstruga, R. (2023) Site-specific analysis reveals candidate cross-kingdom small RNAs, tRNA and rRNA fragments, and signs of fungal RNA phasing in the barley–powdery mildew interaction. *Molecular Plant Pathology*, 24, 570–587. Available from: https://doi.org/10.1111/mpp.13324